MATHEMATICAL MODELING OF THE POLLUTED TROPOSPHERE

John H. Seinfeld
California Institute of Technology
Pasadena, California

INTRODUCTION

The purpose of this paper is to provide an overview of the general problems involved in mathematical modeling of the polluted troposphere (principally the urban atmosphere). The paper is divided into two basic sections:

(1) Fundamentals of air quality models

(2) Aerosol processes in the polluted troposphere

The first section is essentially a review of the major elements of mathematical models. The second section consists of a development of a model capable of predicting the transformation of gaseous material to particulate material in the urban atmosphere and urban plume.

FUNDAMENTALS OF AIR QUALITY MODELS

All conventional atmospheric diffusion models are based on the equation of conservation of mass:

$$\frac{\partial c_i}{\partial t} + u\frac{\partial c_i}{\partial x} + v\frac{\partial c_i}{\partial y} + w\frac{\partial c_i}{\partial z} = D_i\left(\frac{\partial^2 c_i}{\partial x^2} + \frac{\partial^2 c_i}{\partial y^2} + \frac{\partial^2 c_i}{\partial z^2}\right) + R_i(c_1, \ldots, c_N, T) + S_i(x,y,z,t) \qquad (1)$$

where t is time; c_i is the concentration of species i; u, v, and w are the fluid velocities in the three coordinate directions x, y, and z; D_i is the molecular diffusivity of species i in air; R_i is the rate of generation (or the negative of the rate of disappearance) of species i by chemical reactions at temperature T; and S_i is the rate of injection of species i into the fluid from sources.

Substituting the usual mean and fluctuating terms into equation (1) and averaging the resulting equation over the ensemble of flows result in the equa-

tion governing the ensemble average concentration $\bar{c}_i$. In atmospheric applications, the molecular diffusion term is negligible when compared with that representing advective transport. Thus, by neglecting the contribution of molecular diffusion, the equation for $\bar{c}_i$ becomes

$$\frac{\partial \bar{c}_i}{\partial t} + \bar{u}\frac{\partial \bar{c}_i}{\partial x} + \bar{v}\frac{\partial \bar{c}_i}{\partial y} + \bar{w}\frac{\partial \bar{c}_i}{\partial z} + \frac{\partial}{\partial x}\overline{u'c_i'} + \frac{\partial}{\partial y}\overline{v'c_i'} + \frac{\partial}{\partial z}\overline{w'c_i'} = \overline{R_i(c_1, \ldots, c_N, T)} + \bar{S}_i(x,y,z,t) \qquad (2)$$

Equation (2) is a rigorously valid equation for $\bar{c}_i$ (neglecting, of course, molecular diffusion); and, if the variables $\overline{u'c_i'}$, $\overline{v'c_i'}$, $\overline{w'c_i'}$, and any of those arising from R_i are known as functions of space and time, it can be solved in principle to yield $\bar{c}_i$. Unfortunately, $\overline{u'c_i'}$ and so on cannot be measured at all points in an atmospheric flow and cannot be predicted exactly because of the closure problem of turbulent flow. Thus, models must be used for these terms. The model employed in virtually all cases in which atmospheric flows are involved is that based on the concept of eddy diffusivities:

$$\overline{u'c_i'} = -K_H\frac{\partial \bar{c}_i}{\partial x} \qquad \overline{v'c_i'} = -K_H\frac{\partial \bar{c}_i}{\partial y} \qquad \overline{w'c_i'} = -K_V\frac{\partial \bar{c}_i}{\partial z} \qquad (3)$$

The eddy diffusivities K_H and K_V are postulated to be functions of space and time (and not of $\bar{c}_i$ or any of its gradients).

Although there has been some study of the nature of terms of the form $\overline{c_i'^2}$ arising from turbulent chemical reactions, no atmospheric diffusion models for chemically reactive pollutants currently include expressions for these terms. All models neglect the contribution of turbulent concentration fluctuations to the mean reaction rate and employ the approximation,

$$\overline{R_i(c_1, \ldots, c_N, T)} \approx R_i(\bar{c}_1, \ldots, \bar{c}_N, T) \qquad (4)$$

The result of using equations (3) and (4) in equation (2) is the so-called atmospheric diffusion equation (ADE):

$$\frac{\partial \bar{c}_i}{\partial t} + \bar{u}\frac{\partial \bar{c}_i}{\partial x} + \bar{v}\frac{\partial \bar{c}_i}{\partial y} + \bar{w}\frac{\partial \bar{c}_i}{\partial z} = \frac{\partial}{\partial x}\left(K_H\frac{\partial \bar{c}_i}{\partial x}\right) + \frac{\partial}{\partial y}\left(K_H\frac{\partial \bar{c}_i}{\partial y}\right) + \frac{\partial}{\partial z}\left(K_V\frac{\partial \bar{c}_i}{\partial z}\right) + R_i(\bar{c}_1, \ldots, \bar{c}_N, T) + \bar{S}_i(x,y,z,t) \qquad (5)$$

Because the governing equations are nonlinear, they must be solved numerically. Furthermore, the use of numerical techniques generally requires that the modeling region be subdivided into an array of grid cells, where each cell may have horizontal and vertical dimensions on the order of a few kilometers and several tens of meters, respectively. Before the general mass continuity equation can be solved, it must be "filtered" to remove all small-scale variations that the grid cannot resolve, both in the concentration field and in the independent parameters, such as the wind velocities and the eddy diffusivities. The necessary filtering can be accomplished by averaging equation (5) at each point over a volume equivalent to that of a grid cell. This spatial averaging will be denoted by the symbol $\langle\ \rangle$. In addition, equation (5) has been time averaged over an interval equivalent to that used in each step of the numerical solution procedure. Thus, the concentration predictions obtained from equation (5) represent spatially and temporally averaged quantities.

Spatial averaging of equation (5) results in[1]

$$\frac{\partial\langle\bar{c}_i\rangle}{\partial t} + \bar{u}\frac{\partial\langle\bar{c}_i\rangle}{\partial x} + \bar{v}\frac{\partial\langle\bar{c}_i\rangle}{\partial y} + \bar{w}\frac{\partial\langle\bar{c}_i\rangle}{\partial z} = \frac{\partial}{\partial x}\left(K_H\frac{\partial\langle\bar{c}_i\rangle}{\partial x}\right) + \frac{\partial}{\partial y}\left(K_H\frac{\partial\langle\bar{c}_i\rangle}{\partial y}\right) + \frac{\partial}{\partial z}\left(K_V\frac{\partial\langle\bar{c}_i\rangle}{\partial z}\right)$$

$$+ \langle R_i(\bar{c}_i, \ldots, \bar{c}_N, T)\rangle + \langle\bar{S}_i\rangle \qquad (6)$$

As in the case of equation (4), all models employ the approximation,

$$\langle R_i(\bar{c}_i, \ldots, \bar{c}_N, T)\rangle \approx R_i(\langle\bar{c}_i\rangle, \ldots, \langle\bar{c}_N\rangle, T) \qquad (7)$$

Thus, the contribution of subgrid-scale concentration variations to the mean reaction rate are neglected.

The equation that is the basis of all air quality models is obtained by employing equation (7) in equation (6):

$$\frac{\partial\langle\bar{c}_i\rangle}{\partial t} + \bar{u}\frac{\partial\langle\bar{c}_i\rangle}{\partial x} + \bar{v}\frac{\partial\langle\bar{c}_i\rangle}{\partial y} + \bar{w}\frac{\partial\langle\bar{c}_i\rangle}{\partial z} = \frac{\partial}{\partial x}\left(K_H\frac{\partial\langle\bar{c}_i\rangle}{\partial x}\right) + \frac{\partial}{\partial y}\left(K_H\frac{\partial\langle\bar{c}_i\rangle}{\partial y}\right) + \frac{\partial}{\partial z}\left(K_V\frac{\partial\langle\bar{c}_i\rangle}{\partial z}\right)$$

$$+ R_i(\langle\bar{c}_i\rangle, \ldots, \langle\bar{c}_N\rangle, T) + \langle\bar{S}_i\rangle \qquad (8)$$

The validity of the atmospheric diffusion equation relates to how closely the predicted mean concentration $\langle\bar{c}_i\rangle$ corresponds to the true ensemble mean concentration. If the mean velocities $\bar{u}$, $\bar{v}$, and $\bar{w}$ and the source emission

[1]By virtue of the manner in which they are determined, $\bar{u}$, $\bar{v}$, and $\bar{w}$ are assumed to represent spatially averaged quantities.

rate S_i are known precisely at all points as a function of time, then, for an inert species, the only source of a discrepancy between the predicted and true mean concentrations is the eddy diffusivity model for the turbulent fluxes. If the true ensemble mean velocities and concentrations are known for an atmospheric flow, then it is relatively straightforward to assess the validity of equation (8) for specified forms of K_H and K_V. Unfortunately, for any atmospheric flow, the ensemble mean velocities and concentrations can never be computed since the atmosphere presents only one realization of the flow at any time. (Of course, for a statistically stationary flow, ensemble averages can be replaced by time averages. The atmosphere is, however, seldom in a stationary condition for any appreciable period of time.) Because the true mean velocities and source emission rates that are required to solve equation (8) and the true mean concentration with which the solution of equation (8) is to be compared are not available in general, an unambiguous measure of the validity of equation (8) for any particular flow cannot be obtained.

Accuracy evaluation refers to the agreement between model predictions and observations for a model based on a perfectly sound principle; thus, accuracy evaluation is an assessment of the error introduced by inaccuracies of the input information.[2] Whereas an assessment of model validity is very difficult to obtain, accuracy evaluations can be made from estimates of the errors associated with the input information and from numerical sensitivity tests to determine the impacts of such errors on model predictions. Unlike verification and accuracy evaluation, direct determination of the validity of a model is extremely difficult to accomplish because the requisite exact data on emissions, meteorological variables, and air quality are neither available nor easy to obtain. It is therefore necessary to rely on combinations of verification and accuracy-evaluation studies in order to judge the adequacy of a model. By necessity, this approach is adopted here.

Table I summarizes the sources of invalidity and inaccuracy of equation (8). The sources of invalidity cannot be directly assessed for the reasons just stated. The sources of inaccuracy, on the other hand, can be assessed through verification and accuracy-evaluation studies.

The inputs needed to solve the atmospheric diffusion equation together with possible sources of error in those inputs are given in table I. In each instance unless the actual value of the input is known, the level of error in that input can only be estimated. From the standpoint of the effect of errors on the predictions of the equation, joint consideration must be given to the level of uncertainty in each input parameter and the sensitivity of the predicted concentration to the parameter. Uncertainty relates to the possible error in the parameter from its true value, and sensitivity refers to the effect that this variation in the parameter has on the solution of the equation. A parameter

[2]Another term often used in connection with model evaluation is "verification," referring to the agreement between predictions and observations for the specific case in which the observations used for verification were taken from the same pool of data used to develop the input information for the model. Verification contains elements, therefore, of both validation and accuracy evaluation. Henceforth, verification studies will be referred to as validation studies in keeping with the prevailing usage.

may have a large uncertainty associated with it but have little influence on the solution. In such a case, effort at reducing the uncertainty in the parameter value may be unwarranted. On the other hand, small uncertainties in a parameter to which the solution is quite sensitive may have a large impact on uncertainties in the predicted concentrations. Thus, both uncertainty and sensitivity must be considered when the accuracy of the atmospheric diffusion equation is evaluated.

Finally, note that discrepancies between predicted and measured concentrations may arise not only because of inaccuracies in input variables but also because concentrations are measured at a point, whereas the model predicts spatially averaged concentrations. Measurement errors may also, of course, contribute to discrepancies between model predictions and data.

Although the validity of the atmospheric diffusion equation cannot be established without question, it is generally accepted that the equation is essentially a valid description of atmospheric transport, mixing, and chemical reaction processes. The major source of invalidity is the eddy diffusivity representation of the turbulent fluxes. However, as long as the eddy diffusivity functions used have been determined empirically under conditions similar to those to which the equation is applied, the equation should be considered valid. The principal problem, therefore, lies with the question of accuracy, namely the effect of uncertain specification of input parameters on the predictions of the model.

Initial and Boundary Conditions

The initial condition for the atmospheric diffusion equation is that the concentration field at the time corresponding to the beginning of the simulation $\langle \bar{c}_i(x,y,z,0) \rangle = \langle \bar{c}_i \rangle_o$. Simulations are normally begun at night or at sunrise, and the $\langle \bar{c}_i \rangle_o$ field at that time is constructed from the station readings. A ground-level interpolation routine and assumptions regarding the vertical variation of the concentrations are required to generate the full $\langle \bar{c}_i \rangle_o$ field from the station data. Because only surface readings are generally available from which to construct a $\langle \bar{c}_i \rangle_o$ field, the most uncertainty is expected in the initial conditions aloft.

The boundary conditions for equation (8) consist of the concentrations upwind of the region, the pollutant fluxes at the ground (the source emissions), and the flux condition at the upper vertical boundary of the region. Concentrations upwind of the modeling region can be estimated if monitoring stations exist at the upwind edge of the airshed. In such a case, uncertainties in these concentrations will be low when a previous time is simulated. The major source of uncertainty in boundary conditions generally arises at the upper vertical boundary. First, the temperature structure, for example, the height of the base of an elevated inversion layer, is not known precisely. Second, the pollutant flux condition at the boundary is also not known precisely. Thus, the major uncertainty in boundary conditions lies in specifying the upper vertical boundary conditions, both the location of the boundary and the species flux condition at the boundary.

Most models depend for their initial and boundary conditions (I.C. and B.C.) on routine air monitoring data. These data are typically interpolated to a fine mesh to provide the surface-level I.C. and the B.C. for the edges of the region. There are obvious problems with this approach:

(1) The monitoring data are often not representative of the concentration levels surrounding a monitoring station (see, for example, Ott and Eliassen (ref. 1)). The nature of this problem is site specific and must be evaluated for each monitoring site within the modeling region.

(2) The monitoring data represent surface-level measurements. All models require the concentration levels above the inversion base as an upper-level B.C. This problem with B.C. can to a certain extent be eliminated by extending the vertical coordinate of the model domain above the inversion so that background levels can be used. If this is not feasible, and depending on the atmospheric condition, a factor of 3 should be considered as the minimal level of uncertainty associated with upper-level boundary conditions. These uncertainty levels can be reduced if upper-level measurements are available. The problem with upper-level I.C. can to a certain extent be eliminated by starting the model well before the time period of interest.

(3) The most serious problem associated with I.C. and B.C. may be uncertainties associated with the monitoring methods themselves. J. Trijonis (personal communication, 1977) has performed a critical review and statistical analysis of the quality of monitoring methods. Based on this work, the precision of the data corrected for interference effects is recommended to be: O_x/O_3 - excellent, NO_x - good (10-percent error), total hydrocarbons - fair, and non-methane hydrocarbons - poor. Of these data, the largest uncertainty is in the non-methane hydrocarbon data which must be further split for validation according to the requirements of the particular chemical mechanism. A minimum of 50-percent uncertainty should be associated with these measurements unless more refined results are available.

In summary, for most models the major uncertainties are associated with the upper-level data (factor of 3) and with the hydrocarbon measurement ($\approx$50 percent). The problem with horizontal boundary conditions can largely be removed by choice of the model boundaries away from strong gradients and pollutant sources. Uncertainties in initial conditions can be minimized by starting the calculation well before the time period of interest.

Meteorology

There are three basic meteorological variables of interest: wind field, mixing depth, and solar insolation. A problem, common to all models, is that sparse and often unrepresentative measurements are used to derive continuous fields over the region. The key question is, "How representative are the interpolated fields of the actual physical processes in the atmosphere?" Roth et al. (ref. 2) in their study of wind measuring stations in the Los Angeles region found that a substantial proportion of the data, taken at identical or adjacent sites at the same time, differed markedly. A 20-percent error in any of the measurements is not uncommon, the uncertainty in the vertical velocity field

being somewhat greater. The basic effect of small perturbations in the wind field is to introduce an artificial diffusion or smoothing process. Larger errors can affect the time-phasing and magnitudes of pollutant peaks at particular locations. Mass-consistent wind fields, derived by objective analysis procedures and appropriate weighting of station data, can substantially reduce the effects of uncertainties. The artificial creation of convergence and divergence zones can be minimized. Some problems still remain however in creating three-dimensional wind fields from very limited amounts of upper-level data. To some extent, errors in these measurements can often mask physically meaningful calculations of vertical velocities.

All models require specification of the mixing depth. In most regions it is only measured, or calculated from temperature profiles, at a very limited number of locations. A 20- to 30-percent error is typical; however, in regions of convergence or strong heating on surface slopes, the accuracy can be much worse. (In view of the fact that concentration predictions are very sensitive to mixing depth, it is vital to use objective analysis procedures that simultaneously couple the calculation of the wind field and inversion base location.)

The accurate specification of the wind field for use by an air quality model is of critical importance. Since numerical solution of the full Navier-Stokes equations has not yet been proven feasible, the common approach for computing a grid of wind vectors is to use the scattered measured values, generally available at hourly intervals.

The calculation of a continuous surface from discrete data points is a problem common to many fields of science. In general, for a given set of discrete data points, a unique solution does not exist, and, therefore, analysis of a given data set by different techniques often results in different fields.

Interpolation of a surface velocity field.- Much has been written on the subject of objective surface field generation from discrete data values. In an early paper, Panofsky (ref. 3) used third-degree polynomials to fit wind and pressure fields for use in weather map construction. The technique was later modified to handle areas with sparse data by Gilchrist and Cressman (ref. 4). Cressman (ref. 5) reported on a procedure for use in pressure-surface height analysis in which each station value was weighted according to its distance r from the grid point in question. Endlich and Mancuso (ref. 6) combined both polynomial fitting and distance weighting in their technique. A least-squares fit to a plane was performed by using the five nearest station values. Shepard (ref. 7) discussed an interpolation technique in which the value at grid point (i,j) was computed from

$$C_{ij} = \frac{\sum_{k=1}^{n} C_k \, W_k(r)}{\sum_{k=1}^{n} W_k(r)} \tag{9}$$

where C_k is the measured value at the kth measuring station and $W_k(r)$ is the weighting function. A direction factor was also included which accounted for shadowing of the influence of one data point by a nearer one in the same direction. The method also included the effect of barriers. If a "detour" of length b(r), perpendicular to the line between the point (i,j) and the kth measuring station, was required to travel around the barrier between the two points, then b(r) was considered to be the strength of the barrier. An effective distance r' was defined by

$$r' = \left[r^2 + b(r)^2\right]^{1/2} \tag{10}$$

If no barrier separated the two points, then $b(r) = 0$. Shenfeld and Boyer (ref. 8) presented a technique similar to that proposed by Endlich and Mancuso. In an attempt to produce reasonable values in regions of sparse data, Fritsch (ref. 9) used a cubic spline technique. He first fit spherical surfaces to the data to obtain an initial field, and then using the splines, he iteratively adjusted these values until convergence was obtained. He compared his technique with that of Cressman by using an idealized data set with a known solution, and the mean error (≈3 percent) was approximately half that of Cressman's. MacCracken and Sauter (ref. 10) used a weighting scheme based on distance r in the computation of the wind fields for use in the air quality simulation model LIRAQ. The weighting scheme chosen was

$$W(r) = \exp(-0.1r^2) \tag{11}$$

This Gaussian weighting scheme was chosen over r^{-2} weighting in order to eliminate the complete dominance of a measuring station located near a grid point.

In summary, interpolation of sparse data on a grid can be accomplished by weighting each data value according to its distance from the point in question or performing a least-squares fit of the data by a polynomial. In the first approach, stations within a "radius of influence" of the grid point are expected to influence that grid point. The grid point value may be influenced by shadowing, barriers, and/or upwind versus crosswind distance. The second method requires minimization of χ^2, the goodness of fit to the data. For a second-degree polynomial, for example,

$$\chi^2 \equiv \sum_{k=1}^{n} (\Delta C_k)^2 = \sum_{k=1}^{n} (C_k - a_1 - a_2x_k - a_3y_k - a_4x_ky_k - a_5x_k^2 - a_6y_k^2)^2 \tag{12}$$

must be a minimum, where C_k is the measured concentration (or wind speed) at point (x_k,y_k). The minimum value of χ^2 can be determined by setting the derivatives of χ^2 with respect to each of the coefficients a_i equal to zero.

Effect of terrain on surface wind field.- The influence of gross terrain features (e.g., mountain ranges) is accounted for by the use of barriers to flow during the wind component interpolation procedure. However, this does not account for local terrain features on the scale of 1 grid length. Each measured wind vector obviously reflects the local terrain surrounding that station. However, the interpolated vector at a nonmeasuring station grid point is the weighted average of several measured vectors and is only partially indicative of its own local terrain. Therefore, following the aforementioned interpolation procedure, a terrain adjustment technique, which is similar to that of Anderson (refs. 11 and 12) except that surface heating is not included, can be used in the wind field calculation.

Within a layer of constant thickness, the flow can be assumed to be approximately two-dimensional. The scale of vertical variability is so much smaller than the horizontal scale that the flow may be considered as a horizontal flow perturbed by vertical disturbances. Therefore, the continuity equation can be written as

$$\int_h^H \nabla \cdot \underset{\sim}{v}_H \, dz = - \int_h^H \frac{\partial w}{\partial z} \, dz \tag{13}$$

where $\underset{\sim}{v}_H$ is the terrain-adjusted surface wind vector, h is the height of terrain, and H is the top of the disturbed layer. If it is assumed that

$$w_H \approx 0$$

since the topographic influence is no longer felt at this altitude and that

$$w_h \approx \underset{\sim}{V}_0 \cdot \nabla h$$

where $\underset{\sim}{V}$ is the velocity resulting from the interpolation procedure, equation (13) can be integrated to

$$(H - h)\nabla \cdot \underset{\sim}{v}_H = \underset{\sim}{V}_0 \cdot \nabla h \tag{14}$$

If it is assumed that the horizontal velocity can be represented by a velocity potential ϕ such that

$$U = \frac{\partial \phi}{\partial x} \qquad V = \frac{\partial \phi}{\partial y} \tag{15}$$

then equation (14) becomes Poisson's equation,

$$\nabla^2\phi = \frac{\underline{V}_0 \cdot \nabla h}{H - h} \tag{16}$$

The resulting field of ϕ values is used to adjust the initial interpolated surface velocity field to reflect the effect of the terrain as follows:

$$\left.\begin{aligned} u &= U_0 + \frac{\partial\phi}{\partial x} \\ v &= V_0 + \frac{\partial\phi}{\partial y} \end{aligned}\right\} \tag{17}$$

Determination of a mass-consistent three-dimensional wind field.- During recent years only a limited number of divergence reduction procedures have appeared in the literature. Endlich (ref. 13) used a point-iterative method to reduce the two-dimensional divergence in a wind field while retaining the vorticity in the original field. His method involved simple adjustment of the velocity components contributing to the divergence at a given point in order to make the divergence zero at that point. An adjustment was made simultaneously to the vorticity equation. The grid was scanned iteratively point by point until the divergence was reduced to a desired level.

Frankhauser (ref. 14) approached the three-dimensional divergence reduction problem from the point of view of measured data errors. On the basis of the assumption that errors in measured horizontal velocity increase with altitude (O'Brien (ref. 15)), he adjusted initial estimates of vertical velocity to account for this. The horizontal velocity at each vertical level was then adjusted by solving for a velocity potential ϕ from

$$\nabla^2\phi = D_R(x,y) \tag{18}$$

where $D_R(x,y)$ is the residual divergence at point (x,y). He computed the new velocity components from equation (17).

More recently, Sherman (ref. 16) devised a procedure for construction of a three-dimensional mass-consistent wind field (MATHEW) by using the variational calculus approach of Sasaki (refs. 17 and 18). The approach involved solution of the following equation:

$$\frac{\partial^2\lambda}{\partial x^2} + \frac{\partial^2\lambda}{\partial y^2} + \frac{\alpha_1^2}{\alpha_2^2}\frac{\partial^2\lambda}{\partial z^2} = -2\alpha_1^2\left(\frac{\partial u_o}{\partial x} + \frac{\partial v_o}{\partial y} + \frac{\partial w_o}{\partial z}\right) \tag{19}$$

where $\lambda(x,y,z)$ is a Lagrange multiplier (or alternatively a velocity potential); u_o, v_o, and w_o are the observed velocity values; α_1 and α_2 are Gauss' precision moduli defined by $\alpha^2 = 1/2\sigma^2$ where σ^2 is the error variance of the observed field. The adjusted velocity components are then calculated from

$$\left.\begin{aligned} 2\alpha_1^2(u - u_o) + \frac{\partial\lambda}{\partial x} &= 0 \\ 2\alpha_1^2(v - v_o) + \frac{\partial\lambda}{\partial y} &= 0 \\ 2\alpha_2^2(w - w_o) + \frac{\partial\lambda}{\partial z} &= 0 \end{aligned}\right\} \tag{20}$$

The technique requires different boundary conditions depending on the terrain; $\lambda = 0$ is appropriate for open, or "flow-through," boundaries, while $\partial\lambda/\partial n$ is used for closed, or "non-flow-through," boundaries. The procedure was tested on a grid of 24 000 grid points by using data from a canyon near Idaho Falls, Idaho. The precision module α_1^2 and α_2^2 were set to 0.5 and 5000, respectively, apparently from empirical tests. The divergence was reduced 12 orders of magnitude, but the execution time, which is dependent upon terrain complexity, was 2 to 5 minutes on a Control Data 7600 computer.

A two-dimensional vertically integrated version of MATHEW was incorporated into the LIRAQ model developed at Lawrence Livermore Laboratory (MacCracken and Sauter (ref. 10)). The model area extended up to the top of the mixed layer. The appropriate equation of continuity used in the model was

$$\frac{\partial h}{\partial t} + \frac{\partial(uh)}{\partial x} + \frac{\partial(vh)}{\partial y} + w = 0 \tag{21}$$

where h is the depth of the mixed layer and w is the vertical velocity which can be thought of as the relative motion between the vertical movement of the top of the mixed layer and the air through the top of the mixed layer. The variational approach yields the following equation which was solved to adjust the divergence:

$$\frac{\partial^2\lambda}{\partial x^2} + \frac{\partial^2\lambda}{\partial y^2} - \left(\frac{\alpha_1{}^2}{\alpha_2{}^2}\right)\lambda = -2\alpha_1{}^2\left[\frac{\partial h}{\partial t} + \frac{\partial (u_o h)}{\partial x} + \frac{\partial (v_o h)}{\partial y} + w_o\right] \tag{22}$$

When this procedure was tested with wind data from the San Francisco Bay area from July 26, 1973, the divergence was reduced from 10^{-1} to approximately 10^{-6}. A value of 10^{-9} was assumed for $\alpha_1{}^2/\alpha_2{}^2$.

Liu and Goodin (ref. 19) adapted the technique of Endlich to a two-dimensional mesoscale wind field. The flow field below the mixed layer was assumed to be vertically integrated. The divergence was adjusted point by point with the capability of holding wind station values fixed. Since vorticity is not important on the mesoscale, this portion of Endlich's procedure was not implemented. The procedure was tested on wind data from Los Angeles on a 40 × 25 grid. The divergence in the field was reduced by about 3 orders of magnitude after 100 iterations while the measured station values were held fixed.

Emission Inventories

The assessment of the level of uncertainty in a particular emission inventory is obviously a substantial undertaking and, most properly, should be carried out when the inventory itself is compiled.[3]

Emissions from each class of source can be characterized according to

(1) Level of spatial resolution

(2) Level of temporal resolution

(3) Source activity or emission factor

The level of spatial resolution achievable is in principle as fine as one desires since the locations of all sources can presumably be specified (although traffic count data may not be available on a street-by-street basis). Temporal emission rates will fluctuate somewhat from day to day. Emissions from some stationary sources may vary with ambient temperature, but these variations are generally known as a function of temperature. The major problem in properly specifying source emissions is uncertainty in emission quantities arising from uncertainties in source activities and emission factors.

Two basic factors are involved in emission specification, the quantity emitted and its composition. Emission compositions are typically estimated

[3]Typical levels of uncertainties in mobile and fixed source activities (e.g., vehicle distance traveled and units of fuel consumed) should be identified. Then, the typical uncertainties in emission factors (e.g., grams of pollutant emitted per vehicle distance traveled and gram of pollutant per unit of fuel consumed) should be combined with the uncertainties in activities to produce net uncertainties in emissions.

from handbooks such as AP-42 (ref. 20). Each table in AP-42 includes a qualitative estimate of the accuracy of the material on a scale that varies from A (excellent) to E (poor). Recent studies aimed at establishing NO_x and SO_2 emission inventories for stationary sources in the South Coast Air Basin have presented estimates of the level of accuracy of the overall inventories (Bartz et al. (ref. 21) and Hunter and Helgeson (ref. 22)). These reports estimate that a ±20-percent uncertainty in the total emissions is reasonable, whereas uncertainties in individual source emissions can range as high as ±300 percent. A compensating factor is that generally the large uncertainties are associated with small absolute emission levels. Mobile source emission estimates depend to a large extent on the quality of the traffic data. The level of uncertainty in the South Coast Air Basin mobile source emissions of NO_x, CO, and SO_2 is probably of the order of ±15 percent.

Probably the most serious emission inventory problems are those associated with hydrocarbon emissions. The level of uncertainty in the stationary source hydrocarbon emissions in the South Coast Air Basin is probably of the order of ±30 percent. Within individual source classes, the uncertainties can be as high as ±100 percent. Mobile source hydrocarbon emission uncertainties have been estimated in the range from 15 to 50 percent. Generally, insufficient information is available concerning the hydrocarbon composition of major hydrocarbon sources. It is necessary to estimate a hydrocarbon breakdown into the four classes. (Aldehydes constitute an important class of reacting species, and virtually nothing is known about aldehyde emissions.) It is difficult to estimate the uncertainty associated with estimated hydrocarbon speciation. From the point of view of predictions, errors in absolute hydrocarbon levels will be more influential on oxidant predictions than will errors in class assignments, because reactivities do not vary enormously for the classes. Thus, uncertainties in hydrocarbon emissions by class, while definitely leading to uncertainties in oxidant predictions, are not deemed as detrimental to accurate oxidant predictions as are uncertainties in hydrocarbon emissions by total level.

Chemical Kinetics

There are essentially two approaches that have been followed in developing kinetic mechanisms for photochemical smog:

(1) Lumped mechanisms: mechanisms in which organic species are grouped according to a common basis such as structure or reactivity. Examples include the mechanisms of Hecht and Seinfeld (ref. 23), Eschenroeder and Martinez (ref. 24), Hecht et al. (ref. 25), MacCracken and Sauter (ref. 10), and Whitten and Hogo (ref. 26).

(2) Surrogate mechanisms: mechanisms in which organic species in a particular class (e.g., olefins) are represented by a single member of that class (e.g., propylene). Examples include the mechanisms of Niki et al. (ref. 27), Demerjian et al. (ref. 28), Dodge (ref. 29), and Graedel et al. (ref. 30).

In general, the surrogate mechanisms tend to be more lengthy than lumped mechanisms because within a surrogate mechanism each individual species is treated as a separate chemical entity. For this reason surrogate mechanisms

have not found wide utility in models that have substantial meteorological treatments because of the computational requirements associated with calculating simultaneous chemistry and transport.

Table II presents a comparison of two lumped mechanisms that are currently employed in air quality models. The SAI and LIRAQ mechanisms, modified versions of the Hecht et al. (ref. 25) mechanism, are included in large-scale urban air quality models. Table II lists all the reactions and associated rate constants that are included in the two mechanisms. The issue of most interest here is which reactions are included in which mechanisms and not the particular rate constant value adopted. (The rate constant values in all mechanisms continually undergo revision as new measurements become available, and several of the constants given in table II have recently been reevaluated.)

From table II, it is clear that, aside from rate constant differences, the two mechanisms are quite similar, even though the interpretation of the lumped organic species varies somewhat between the mechanisms. Differences in rate constants are the result of choices from among available rate constant values and more recent determinations as well as the result of different lumping schemes.

The critical question, of course, in the development of a kinetic mechanism is its accuracy. The assessment of the accuracy of chemical kinetic mechanisms for photochemical smog has received a considerable amount of attention (Hecht and Seinfeld (ref. 23), Niki et al. (ref. 27), Hecht et al. (ref. 25), Demerjian et al. (ref. 28), Dodge and Hecht (ref. 31), Dodge (ref. 29), and Whitten and Hogo (ref. 26)). There are essentially two issues involved in assessing the accuracy of a kinetic mechanism: (1) identification of the major sources of uncertainty, such as inaccurately known rate constants or mechanisms of individual reactions, and (2) evaluation of so-called chamber effects, phenomena peculiar to the laboratory system in which the data are generated for testing of a mechanism.

Predicted concentrations are extremely sensitive to the values of several reaction rate constants. Reactions that are particularly important are those governing the conversion of NO to NO_2 and those that initiate the oxidation of hydrocarbons. Dodge and Hecht (ref. 31) performed a systematic sensitivity analysis of the reactions in the original Hecht-Seinfeld-Dodge kinetic mechanism. The conclusions of the study were compiled in the form of a ranking of the reactions by their "sensitivity-uncertainty" index. This index is an indicator of the combined sensitivity of the mechanism to variations in the reaction rate constant and the experimental uncertainty of the rate constant. Since this study was performed, several rate constant determinations have been significantly improved.

The overall smog formation process as simulated by present mechanisms can be described in terms of two radical pools. One of these pools is the oxygen radical pool; it is associated with NO_2 photolysis and the production of ozone. The other radical pool can be referred to as the peroxy-oxyl radical pool. In this pool, radical transfer reactions convert peroxy radicals to oxyl radicals and vice versa, with the concomitant conversion of NO to NO_2 and oxidation of hydrocarbons. Oxyl radicals are formed when peroxy radicals convert NO to NO_2.

Peroxy radicals are formed when hydroxyl radicals react with hydrocarbons, and hydroperoxy radicals are formed when alkoxyl radicals react with molecular oxygen.

A major problem with simulating experimental smog chamber data is that it is difficult to reproduce the initial rate of hydrocarbon disappearance and the initial rate of conversion of NO to NO_2. This difficulty is often resolved by assuming an initial source of peroxy or oxyl radicals in addition to those formed by the reactions of oxygen atoms with hydrocarbons, for example, by assuming an initial concentration of nitrous acid, which photolyzes and supplies the initial radicals. Whether nitrous acid is initially present in the smog chambers in the amounts assumed is unknown.[4]

Once the pool of peroxy-oxyl radicals is established in a simulation, the radical pool must be maintained, because radical sinks, such as the reaction of hydroxyl radicals with NO_2 or peroxy-peroxy combination reactions, tend to consume more radicals than are produced by NO_2 photolysis and the subsequent reactions of oxygen atoms. The radical concentration is maintained in the mechanism by the photolysis of carbonyl compounds (and, in olefin systems by the ozone-olefin reactions). In some cases it is obvious that too many radicals are present initially and that the maintenance source of radicals in the mechanism is inadequate. It has been speculated that the walls of chambers in some way supply radicals to the peroxy-oxyl radical pool. The effect of such a process would be greatest when the concentration of normal radicals was the lowest - in a low activity and low hydrocarbon experiment. That the walls may be supplying radicals is supported by the similar need for a high initial HONO concentration (relative to equilibrium).

Kinetic mechanisms must be able to predict the photolysis rates of pollutants that absorb ultraviolet light. From Beer's law, in an optically thin medium the first-order rate constant governing the photolysis rate of a compound is given by

$$k = \frac{1}{(\lambda_2 - \lambda_1)} \int_{\lambda_1}^{\lambda_2} \phi(\lambda)\ I_o(\lambda)\ \varepsilon(\lambda)\ d\lambda$$

where

$I_o(\lambda)$ incident light intensity distribution

$\varepsilon(\lambda)$ extinction coefficient

---

[4]There is evidence that nitrous acid is found during the loading of smog chambers (Chan et al. (ref. 32)). The amount required to simulate University of California, Riverside experiments was found by Whitten and Hogo (ref. 26) to be generally about one-third of the equilibrium concentration of nitrous acid that could form from the initial concentrations of NO, NO_2, and H_2O. Whether the walls of the smog chamber are an important source of initial radicals is unknown.

$\phi(\lambda)$ primary quantum yield

λ_1, λ_2 wavelength limits of the light reaching the urban atmosphere

In smog chamber simulations, the photolysis rate is usually expressed in terms of k_1, the rate constant for NO_2 photolysis. From this, with information on $I_o(\lambda)$, $\epsilon(\lambda)$, and $\phi(\lambda)$, photolysis rates of other species can be predicted. Considerable uncertainty exists in the measurement of $\phi(\lambda)$ for certain species. For instance, the photolysis of ozone can be important in the formation of OH radicals. In the wavelength region of interest, the primary quantum yields for the processes

$$O_3 + h\nu \rightarrow O_2(^1\Delta) + O(^1D)$$

$$O_3 + h\nu \rightarrow O_2(^1\Sigma) + O(^3P)$$

are still uncertain. While extinction coefficients are relatively easy to measure in the laboratory for most species, quantum yield measurements can be exceedingly difficult.

Another important photochemical process is the formation and subsequent reaction of excited states. The rates of thermal reactions can be enhanced by several orders of magnitude if one or more of the reactants are vibrationally or electronically excited. For instance, while ground-state $O(^3P)$ atoms are unreactive toward such species as H_2, H_2O, and N_2O, singlet oxygen, $O(^1D)$, reacts rapidly. Similarly, the oxidation of SO_2 in clean air probably takes place by the reaction of triplet SO_2 ($^3SO_2$) formed by the absorption of ultraviolet light by ground-state SO_2 followed by internal energy transfer processes; $^3SO_2$ may also be considerably more reactive toward hydrocarbons than the ground-state SO_2. Unfortunately, both the formation and the reaction mechanisms of most electronically excited species are highly uncertain.

As noted previously, the characteristics of the chamber must be accounted for, since mechanisms must be validated with smog chamber data. Some of the specific effects or characteristics that must be considered are the spectral distribution and absolute intensity of the photolyzing lamps, the adsorption, desorption, and chemical reaction of species on the walls, the initial loading of impurity species in the chamber on the walls or in the gas, and the effects of leakage, sampling, and possible temperature variations during the run. Of these effects, probably the most important are the properties of the photolysis lamps. Photolysis rates of absorbing species cannot be predicted with accuracy if $I_o(\lambda)$, the incident light intensity distribution, is not known with accuracy. This information must be coupled with the absolute rate of photolysis of at least one species such as NO_2 to compute the appropriate photolysis rate constants.

Also important is the characterization of the initial contaminant loading in the chamber. When mechanisms overpredict the length of the induction period in which radical concentrations are initially building up, it may be due to the

presence of an absorbing species either in the gas phase or on the walls which photolyzes. Actual measurement of the species accounting for these effects is complicated by their low concentrations.

When these effects are not adequately characterized, one usually begins by parameterizing the NO_2 photolysis rate constant k_1, the initial concentration of trace photolyzable species such as HONO, and the wall adsorption rate of ozone. If still less is known about the experimental situation, the value of simulating the data becomes questionable.

The third major set of unknowns in simulating laboratory systems concerns the reactions which take place heterogeneously, either on the walls or on aerosols. Many reactions are thought to take place heterogeneously. Among the most important are the reactions,

$$NO + NO_2 + H_2O \rightleftarrows 2HONO$$

$$NO_2 + NO_3 + H_2O \rightleftarrows 2HONO_2$$

which produce nitrous acid and nitric acid. Evidence for the heterogeneous nature of these processes comes from the strong dependence of measured rate constants on the reactor surface-to-volume ratio. (The disappearance of SO_2 in smog chamber experiments also seems to have a strong heterogeneous component either as a result of reactions in droplets or the wall-catalyzed formation of polymeric sulfur-oxygen species which remain on the walls as films.) Recent work has shown that certain long-lived free radicals such as HO_2 can be lost to particles at appreciable rates. Diffusion and subsequent loss of radicals to reactor walls occur constantly, but these processes do not affect the homogeneous chemistry appreciably. Heterogeneous processes, in general, are difficult to account for in kinetic mechanisms and are usually ignored.

In summary, virtually every reaction occurring in an atmospheric system is subject to some degree of uncertainty, whether in the rate constant or the nature and quantity of the products. In evaluating a mechanism, the customary procedure is to compare the results of smog chamber experiments, usually in the form of concentration-time profiles, with simulations of the same experiment using the proposed mechanism. A sufficient number of experimental unknowns exist in all such mechanisms that the predicted concentration profiles can be varied somewhat by changing rate constants (and perhaps mechanisms) within accepted bounds. The inherent validity of a mechanism can be judged by evaluating how realistic the parameter values used are and how well the predictions match the data.

Numerical Analysis

A major area that must be considered is the numerical approximations required to solve the mathematical model. Complex numerical schemes are required to solve the three-dimensional, coupled, nonlinear, parabolic partial

differential equations that result from the atmospheric diffusion equation. The choice of numerical methods to be used in the approximated model are important factors that influence the accuracy and economy of the solution. In most cases, spatial and temporal discretization introduces additional averaging and a loss of characterization of subgrid-scale processes. This problem can be corrected, to some extent, by the use of subgrid-scale models, but they must be augmented by careful analysis of the influence of grid size and time step on the accuracy of the results.

A common source of inaccuracy in the solution of equation (8) is numerical truncation errors in the approximation of the advection terms. These should be minimized by using, for example, high-order schemes such as the zero average phase error technique of Fromm (ref. 33) or the sign preserving SHASTA method of Boris and Book (ref. 34). The requirements for high-order accuracy must be balanced with computer resource requirements.

The accuracy of numerical schemes can, in principle, be evaluated by performing numerical experiments with problems of known analytic solutions. Tests can be used to assess the effects of numerical diffusion and the influence of dispersion on phase errors. Numerical dissipation dominates in first-order difference schemes and tends to reduce the amplitude of concentration peaks, while in second-order approximations, dispersion at high wave numbers becomes the most serious problem. Dispersion is common to all methods but dissipation is absent from time-centered schemes. A common test is the Crowley (ref. 35) "color" problem in which a conical distribution of a scalar quantity is advected by a circular velocity field.

Special consideration must be given to the character of the chemical terms and their numerical properties. Solution of the stiff system of ordinary differential equations that often arises requires the use of Newton iteration or variable order methods like DIFSUB (Gear (ref. 36)). Stability requirements must be carefully evaluated with attention given to the disparity of the temporal scales of the processes being modeled.

Assessment of Accuracy of Models for Photochemical Oxidant

Inaccuracies in the predictions of models arise from two sources: (1) lack of complete understanding of atmospheric physics and chemistry and (2) inaccuracies in input data due to incomplete data bases.[5] In terms of understanding of atmospheric physics and chemistry, the primary concerns are accurate treatment

[5]Liu and Seinfeld (ref. 37) showed that an important technical limitation of models is that the diffusion equation is difficult to solve accurately. In particular, conventional finite-difference techniques introduce a pseudodiffusion effect as a result of poor treatment of advective transport. For example, relative errors of as much as 50 percent could be generated by using the numerical method in the 1973 version of the SAI model. In general, the developers of all models have recognized this numerical problem and have implemented special techniques aimed at alleviating the undesired effect. Now, discrepancies between predictions and measurements are mainly attributable to errors introduced in the formulation of and inputs to the model.

of advection, turbulent diffusion, and chemistry. Although advection is a complicated process that has yet to be treated definitively, horizontal advection can be incorporated correctly. Turbulent diffusion (primarily in the vertical direction) may be treated inaccurately because of a lack of complete understanding of the process. Nevertheless, most parameterizations of the vertical eddy diffusivity provide an appropriate rate of vertical mixing. Inaccuracies in the understanding of turbulent diffusion, therefore, do not appear to pose a serious problem with respect to the accuracy of predictions. The greatest source of uncertainty is in the understanding of the chemical transformations that lead to ozone formation. These processes have been studied for many years in smog chambers, and several kinetic mechanisms have been proposed that provide concentration predictions that agree at least qualitatively with the experimental results. Yet, all the significant chemical reactions may not have been identified, and furthermore, the rate constants for many reactions believed to be important are not known very accurately. Finally, it has not been established conclusively that a mechanism validated with smog chamber data accurately represents actual atmospheric chemical processes. Initial and boundary conditions and source emissions lead to inaccuracies in predictions because of uncertainties due to an incomplete data base.

Few available studies present detailed analyses of the sensitivity of model predictions to changes in input parameters. The importance of sensitivity results cannot be overemphasized. Practically, they are of value in assessing the level of detail and accuracy required in model input parameters or the effects of uncertainties on predictions. The only extensive, published sensitivity study is that of Liu et al. (ref. 38) for the SAI model.[6] Most of their findings are summarized in the following table:

RANKING OF THE RELATIVE IMPORTANCE OF THE INPUT PARAMETERS (SAI MODEL)

Variable	Importance[a] of variable to prediction of concentration of -			
	CO	NO	O_3	NO_2
Wind speed	A	A	A	A
K_H	D	D	D	D
K_V	C	C	C	C
Mixing depth	B	B	B	B
Radiation intensity	D	A	A	B
Emission rate	B	A	B	B

[a]Importance is indicated by a scale from A (most important) to D (least important).

[6]For a description of the SAI model see Reynolds et al. (refs. 39 to 42) and Roth et al. (refs. 2 and 43).

The effect of varying boundary and initial conditions in the 1973-version of the SAI model was reported by Demerjian (ref. 44). Average ozone concentration maps for the Los Angeles basin between the hours of 1:00 and 2:00 p.m. were presented for the base case and the case of boundary conditions reduced by 50 percent. Only minor differences were found at the eastern and northern edges of the basin where the maxima occur, but significant differences were observed at the western and central portions of the basin. The initial conditions in addition to the boundary conditions were reduced by 50 percent. Reduction in the predicted ozone levels at the northern and eastern edges of the basin was found to be of the order of 20 to 30 percent corresponding to the reduced initial conditions.

AEROSOL PROCESSES IN THE POLLUTED TROPOSPHERE

Atmospheric pollutants in an urban airshed exist in both gaseous and particulate phases. In addition to direct emissions of both phases of pollutants (primary pollutants), there exist transformation processes from one gaseous pollutant to another and from gaseous to particulate pollutants (secondary pollutants). Considerable work has been done on the development of mathematical models describing the relationship between sources and ambient levels of gaseous pollutants, including the complex chemistry describing the formation of secondary gaseous pollutants. The development of models describing the evolution of atmospheric aerosols is the next step in the process of attempting to understand the physics and chemistry of the polluted atmosphere.

Dynamic Equation Governing Aerosol Behavior

Presented first are the dynamic equation governing aerosol behavior, with emphasis on application to an urban airshed, and a discussion of the mechanism that each term represents.

The derivation of the general dynamic equation has been presented elsewhere (Chu and Seinfeld (ref. 45)). The general dynamic equation governs the size-composition distribution function for the atmospheric aerosol. Since there exists no experimental means for measuring this distribution function, only the equation governing an integral moment of the general equation, the particle size distribution function, will be presented and discussed here.

If $n(D_p, \underset{\sim}{r}, t)$ is the instantaneous distribution of particles by particle diameter (cm^{-4}), then the general dynamic equation governing $\bar{n}(D_p, \underset{\sim}{r}, t)$, the mean size distribution function, is[7]

[7]Stochastic coagulation and condensation terms have been neglected (see Seinfeld and Ramabhadran (ref. 46)).

$$\frac{\partial \bar{n}}{\partial t} + \sum_{i=1}^{3} \frac{\partial}{\partial r_i}\left(\bar{u}_i \bar{n}\right) + \frac{\partial}{\partial D_p}\left(\bar{I}_o \bar{n}\right) - u_s \frac{\partial \bar{n}}{\partial r_3}$$

$$= \sum_{i=1}^{3} \frac{\partial}{\partial r_i}\left(K_{ii} \frac{\partial \bar{n}}{\partial r_i}\right) + \int_0^{D_p/2^{1/3}} \beta\left[(D_p^3 - \tilde{D}_p^3)^{1/3}, \tilde{D}_p\right] \bar{n}\left[(D_p^3 - \tilde{D}_p^3)^{1/3}, \underset{\sim}{r}, t\right]$$

$$\times \bar{n}(\tilde{D}_p, \underset{\sim}{r}, t) \frac{D_p^2}{(D_p^3 - \tilde{D}_p^3)^{2/3}} d\tilde{D}_p - \int_0^{\infty} \beta(D_p, \tilde{D}_p)\ \bar{n}(D_p, \underset{\sim}{r}, t)\ \bar{n}(\tilde{D}_p, \underset{\sim}{r}, t)\ d\tilde{D}_p$$

$$+ S_0(D_p, t) + S_1(D_p, \underset{\sim}{r}, t) \qquad (23)$$

where

β	coagulation coefficient for particles of diameter D_p and $\tilde{D}_p$, cm^3-sec^{-1}
K_{ii}	turbulent diffusivity in ith direction, cm^2-sec^{-1}
I_o	rate of change of aerosol particle diameter from condensation, cm-sec^{-1}
r_i	spatial variable in ith direction, cm
S_0	rate of homogeneous nucleation, cm^{-4}-sec^{-1}
S_1	rate of particulate sources, cm^{-4}-sec^{-1}
$\bar{u}_i$	mean velocity in ith direction, cm-sec^{-1}
u_s	settling velocity, cm-sec^{-1}

The terms on the left-hand side of equation (23) represent accumulation, convection, and growth by condensation and settling. The terms on the right-hand side represent turbulent diffusion (Brownian diffusion has been neglected), coagulation, nucleation, and particulate sources. With appropriate boundary conditions, equation (23) represents the most general form of the dynamic equation for an aerosol the chemical composition of which is a unique function of its size, spatial position, and time.

If equation (23), with appropriate boundary conditions, could be solved numerically for conditions typifying a general urban airshed, the aerosol model would be complete. Understanding of many components of the model is inadequate, however, the most important components being primary particulate emissions inventories, the chemical mechanisms of gas-to-particle conversion, and rates of homogeneous nucleation. A preliminary step in proceeding toward a general urban aerosol model requires both a closer examination of the system as a whole and a more detailed look at the specific mechanisms present in equation (23).

Figure 1(a) is a diagram describing the interaction between gaseous and particulate pollutants. The additional complexity of the particulate system over the gaseous system becomes readily apparent. From primary emissions of gaseous pollutants, the chemical composition and size of an aerosol particle is altered by diffusion and condensation of vapor species and by absorption of primary gaseous pollutants. Once absorbed, dissolved vapors may participate in heterogeneous reactions. This process of condensation or absorption takes place on primary aerosols, background particles such as soil dust and marine aerosol, on stable nuclei formed by homogeneous nucleation, or on particles formed by coagulation of any of the above particulate species.

This dynamic process of chemical change, particle growth by condensation and coagulation, and removal and replenishment of particles takes place as the aerosol mass is transported through an urban airshed. Additional physical removal mechanisms (deposition, settling, washout, and rainout) affect the aerosol distribution.

The distribution of aerosols in an atmosphere or smog chamber is affected by different mechanisms, depending upon the aerosol number concentration, the gaseous compounds present, and whether the system of interest is open or closed. For example, the description of the evolution of an aerosol distribution in the immediate vicinity of a particulate source must generally include the coagulation mechanism, whereas the description of an "aged" aerosol far downwind from primary sources can usually neglect coagulation. Table III outlines various atmospheric aerosol-particulate systems and the important mechanisms for each system.

Before any system can be described in detail, the first and most important step is to close all mass and energy balances on the system. In the atmosphere, ambient conditions are such that the assumption of constant temperature, while strictly incorrect, can be made without introducing significant errors. Hence, the mass or material balance is the important equation to be considered first.

The next section is concerned with such a material balance of gas-phase and particulate pollutants. In that section, an attempt is made to answer the question, "By utilizing simple mechanisms for source, conversion, and removal rates in the general mass balance equation for particulate pollutants and gaseous precursors, can the ambient levels of these pollutants measured in urban airsheds be accounted for?"

Figure 1(b) outlines the relationship of the next section to the processes described in the general dynamic equation. The processes within the dashed line are replaced by a simple model of gas-to-particle conversion with no particle size dependence. As can be seen, the full system is considered, but certain detailed descriptions of the general equation are replaced with "black box" substitutes. These surrogate representations seek to describe the salient features of the mechanism involved while ignoring the detail of the mechanism. The mechanisms of gas-to-particle conversion are replaced by a simple first-order rate of conversion from gaseous pollutants to total particulate mass. By retaining the basic mechanisms of advection, diffusion, and removal of both gases and particulates, the question of accountability for reported ambient levels of pollutants can be answered.

Model for Predicting Gas-to-Particle Conversion

Most available mathematical models for the steady-state or dynamic behavior of air pollutants apply to gaseous pollutants (either chemically inert or reactive) or to particulate matter that may be considered chemically inert. One of the important atmosphere phenomena that requires elucidation is the conversion of air pollutants from gaseous form to particulate form. For example, of particular interest is the so-called urban plume, wherein sulfur dioxide is converted to particulate sulfate, nitrogen oxides to particulate nitrate, and hydrocarbons to particulate organic material. Several recent studies have been reported in which measurements (usually airborne) have been carried out downwind of large urban complexes in order to obtain material balances on gaseous and particulate pollutants (Haagenson and Morris (ref. 47), Stampfer and Anderson (ref. 48), and Breeding et al. (refs. 49 and 50)). A goal of these studies is to determine the relative roles of transport, conversion of gaseous pollutants to particulate pollutants, and removal on the overall pollutant material balance downwind of a major urban source.

In the analysis of urban plume data, it is desirable to have a mathematical model capable of describing the behavior of both gaseous and particulate pollutants and their interrelations. Eventually such a model would include both gaseous and particulate phases with detailed treatments of gas-phase and particulate-phase chemistry, as well as size distributions of the particles. However, before attempting to develop a model of full complexity, it is desirable to formulate a "first-order" model, one that contains all the major mechanisms influencing the airborne concentrations of gaseous and particulate pollutants but one that does not include the details of atmospheric chemistry and particle size distributions. The processes to be included are advection, turbulent diffusion, conversion of gaseous species to particulate material, settling, deposition, washout, and rainout. Such a first-order model is in essence a material balance, designed to provide estimates of the fraction of pollutants that still remain airborne at a certain distance downwind of a city and the fraction that has been removed by deposition and gas-to-particle conversion. The object of this study is to develop such a model. It is hoped that the model presented in this section will subsequently prove to be a convenient tool in the analysis of airborne urban plume pollutant flux measurements.

Although a dynamic model is desirable, a steady-state model will enable one to assess whether all the major mechanisms are accounted for in analyzing data on urban pollutant fluxes. The model will be restricted to scales of transport over which the atmospheric diffusion equation is applicable, that is, to problems on the mesoscale. "Long-range" transport is not considered because of the recognized inadequacy of the atmospheric diffusion equation in describing macroscale transport. (For consideration of long-range transport, the reader is referred to Bolin and Persson (ref. 51).) There exist a variety of numerical models (numerical solutions of the atmospheric diffusion equation) capable of simulating the transport and removal of air pollutants, for example, Belot et al. (ref. 52). However, there is considerable attractiveness in an analytical model that does not require numerical solution of the atmospheric diffusion equation. In previous work of this nature, Heines and Peters (ref. 53) have presented analytic steady-state solutions for gas-phase pollutants with no deposition or depletion due to reaction. Scriven and Fisher (ref. 54) have presented

a solution to the steady-state, two-dimensional atmospheric diffusion equation including deposition and first-order removal.

Presented in this paper is a new solution to the steady-state, three-dimensional atmospheric diffusion equation including settling, deposition, and first-order removal and conversion of gaseous pollutants to particulate pollutants. The main purpose of the model is to enable the carrying out of overall material balance calculations for the gaseous and particulate phases in the urban atmosphere and in the urban plume. The application of the model to the Los Angeles atmosphere and to the Los Angeles urban plume can be found in Peterson and Seinfeld (ref. 55). A study of that type not only provides estimates of the relative roles of transport and removal mechanisms but also is a necessary prerequisite to more detailed modeling studies involving gases and particles.

Formulation of the model.- The mean concentration $c(x,y,z)$ of a gaseous pollutant or of a primary particulate pollutant under conditions in which the mean wind is aligned with the x-axis and in which a first-order removal process exists can be described by the atmospheric diffusion equation. (Bars over c are omitted for convenience.)

$$\bar{u}\frac{\partial c}{\partial x} - w_s\frac{\partial c}{\partial z} = \frac{\partial}{\partial y}\left(K_H\frac{\partial c}{\partial y}\right) + \frac{\partial}{\partial z}\left(K_V\frac{\partial c}{\partial z}\right) - kc \tag{24}$$

where $\bar{u}$ is the mean wind speed in the x-direction, w_s is the settling velocity (nonzero if c represents the concentration of particulate matter), K_H and K_V are the horizontal and vertical eddy diffusivities, and k is the first-order rate constant for removal of the species. The term kc may account for conversion of gaseous pollutants to particulate material (as long as the process may be represented approximately as first order) or for the removal of either gases or particles by rainout and washout.

The following boundary conditions to equation (24) are considered. The source is taken to be a point source of strength Q_1 ($g\text{-}sec^{-1}$) located at $x = 0$, $y = 0$, $z = z_s$. (From the solution for this elevated point source, solutions can be constructed for all other types of sources of interest.) Thus, the $x = 0$ boundary condition is

$$c(0,y,z) = \frac{Q_1}{\bar{u}}\,\delta(y)\,\delta(z-z_s) \tag{25}$$

where $\delta(\ )$ is the Dirac delta function.

At infinite lateral distance, the concentration approaches zero:

$$c(x,y,z) = 0 \qquad (y \to \pm\infty) \tag{26}$$

An elevated inversion base which inhibits vertical turbulent mixing is assumed to exist at $z = H_a$:

$$\frac{\partial c}{\partial z} = 0 \qquad (z = H_a) \qquad (27)$$

Finally, the pollutant may be removed across a layer at height $z = z_a$ through deposition with a deposition velocity v_d:

$$K_V \frac{\partial c}{\partial z} + w_s c = v_d c \qquad (z = z_a) \qquad (28)$$

Note that the lower boundary conditions was selected at z_a, the height corresponding to that at which a deposition velocity may have been measured. (A typical value of z_a is 1 meter.) For simplicity, K_H and K_V may be taken as constants. The problems associated with this assumption are well known (Monin and Yaglom (ref. 56)). Nevertheless, it is not deemed necessary to include the additional complication of spatially dependent K_H and/or K_V.

It is convenient to cast the problem in dimensionless form. To do so, the following dimensionless spatial variables are defined:

$$X = \frac{K_V x}{\bar{u} H^2} \qquad Y = \frac{y}{H} \qquad Z = \frac{z - z_a}{H} \qquad (29)$$

where $H = H_a - z_a$. In addition, the dimensionless concentration is defined as

$$C = \frac{\bar{u} H^2 c}{Q_1} \qquad (30)$$

With these definitions, equations (24) to (28) become

$$\frac{\partial C}{\partial X} - W \frac{\partial C}{\partial Z} = \beta \frac{\partial^2 C}{\partial Y^2} + \frac{\partial^2 C}{\partial Z^2} - \alpha C \qquad (31)$$

$$C(0, Y, Z) = \delta(Y)\ \delta(Z - Z_s) \qquad (32)$$

$$C(X,Y,Z) = 0 \qquad (Y \to \pm\infty) \qquad (33)$$

$$\frac{\partial C}{\partial Z} = 0 \qquad (Z = 1) \qquad (34)$$

$$\frac{\partial C}{\partial Z} = (N - W)C \qquad (Z = 0) \qquad (35)$$

where $W = w_s H/K_V$, $\beta = K_H/K_V$, $\alpha = kH^2/K_V$, and $N = v_d H/K_V$ (N represents the dimensionless deposition velocity, or mass transfer coefficient).

The details of the solution are found in Peterson (ref. 57). The solution of equations (31) to (35) is

$$C(X,Y,Z) = \frac{1}{2\sqrt{\beta\pi X}} \exp(-\alpha X) \exp\left(-\frac{Y^2}{4\beta X}\right) \exp\left(-\frac{WZ}{2}\right)\left[\sum_{n=1}^{\infty} a_n \Phi_n^{(1)}(Z) \exp\left(-\mu_n^{(1)} X\right) + \sum_{m=1}^{M} c_m \Phi_m^{(2)}(Z) \exp\left(-\mu_m^{(2)} X\right)\right] \qquad (36)$$

where

$$\Phi_n^{(1)}(Z) = \cos(\gamma_n Z) + \delta_n \sin(\gamma_n Z) \qquad (37)$$

$$\Phi_m^{(2)}(Z) = \exp(\theta_m Z) - \tau_m \exp(-\theta_m Z) \qquad (38)$$

$$\mu_n^{(1)} = \gamma_n^2 + \left(\frac{W}{2}\right)^2 \qquad (39)$$

$$\mu_m^{(2)} = \left(\frac{W}{2}\right)^2 - \theta_m^2 \qquad (40)$$

$$\delta_n = \frac{N - W/2}{\gamma_n} \qquad (41)$$

$$\tau_m = \frac{N - W/2 - \theta_m}{N - W/2 + \theta_m} \tag{42}$$

$$a_n = \frac{\exp(WZ_s/2)\left[\cos(\gamma_n Z_s) + \delta_n \sin(\gamma_n Z_s)\right]}{\frac{1}{2}(1 + \delta_n{}^2) + (1 - \delta_n{}^2)\sin(2\gamma_n)/4\gamma_n + \delta_n \sin^2\gamma_n/\gamma_n} \tag{43}$$

$$c_m = \frac{\exp(WZ_s/2)\left[\exp(\theta_m Z_s) - \tau_m \exp(-\theta_m Z_s)\right]}{\left\{\exp(2\theta_m) - 1 + \tau_m{}^2\left[1 - \exp(-2\theta_m)\right]\right\}/2\theta_m - 2\tau_m} \tag{44}$$

and where the eigenvalue relations are

$$\frac{\tan \gamma_n}{\gamma_n} = \frac{N - W}{\gamma_n{}^2 + \frac{W}{2}\left(N - \frac{W}{2}\right)} \qquad (n = 1, 2, \ldots) \tag{45}$$

and

$$\exp(2\theta_m) = \left(\frac{N - W/2 - \theta_m}{N - W/2 + \theta_m}\right)\left(\frac{W/2 + \theta_m}{W/2 - \theta_m}\right) \qquad (m = 1, 2, \ldots, M) \tag{46}$$

The finite sum (m = 1 to M) in equation (36) arises from the finite number (M) of roots of equation (46), whereas the infinite sum in equation (36) arises from the infinite number of roots of equation (45). Whereas equations (43) and (44) are analytically exact, their inclusion in the solution (eq. (36)) does not yield a convergent expansion because the coefficients arise from the eigenfunction expansion of the delta function $\delta(Z-Z_s)$. For computational purposes, it is necessary to approximate the delta function by a more well-behaved function and then represent this function by an eigenfunction expansion. This procedure and the resultant equations for a_n and c_m are given in Peterson and Seinfeld (ref. 55).

Equation (36) can be extended to include L point sources, each of strength Q_i located at (X_i, Y_i, Z_s) for $i = 1, 2, \ldots, L$:

$$C(X,Y,Z) = \frac{1}{2\sqrt{\beta\pi}} \exp\left(-\frac{WZ}{2}\right) \sum_{i=1}^{L} \hat{Q}_i \, U(X-X_i) \, \exp\left[-\frac{(Y-Y_i)^2}{4\beta(X-X_i)}\right] \frac{\exp\left[-\alpha(X-X_i)\right]}{\sqrt{X-X_i}}$$

$$\times \left\{ \sum_{n=1}^{\infty} a_n \, \Phi_n^{(1)}(Z) \, \exp\left[-\mu_n^{(1)}(X-X_i)\right] \right.$$

$$\left. + \sum_{m=1}^{M} c_m \, \Phi_m^{(2)}(Z) \, \exp\left[-\mu_m^{(2)}(X-X_i)\right] \right\} \tag{47}$$

where $\hat{Q}_i = Q_i/Q_1$, and $U(X-X_i)$ is the unit step function,

$$U(X-X_i) = \left\{ \begin{array}{ll} 0 & (X < X_i) \\ 1 & (X \geqq X_i) \end{array} \right\} \tag{48}$$

For L area sources, each of strength q_i $(g\text{-}m^{-2}\text{-}sec^{-1})$ located in the rectangular regions, $X_{ia} \leqq X \leqq X_{ib}$, $Y_{ia} \leqq Y \leqq Y_{ib}$, the mean concentration is given by

$$C(X,Y,Z) = \frac{1}{2} \exp\left(-\frac{WZ}{2}\right) \sum_{i=1}^{L} \hat{q}_i \, U(X-X_{ia}) \left[\sum_{n=1}^{\infty} a_n \, \Phi_n^{(1)}(Z) \left(I_n^{(1)} - I_n^{(2)}\right) \right.$$

$$\left. + \sum_{m=1}^{M} c_m \, \Phi_m^{(2)}(Z) \left(I_m^{(3)} - I_m^{(4)}\right) \right] \tag{49}$$

where $\hat{q}_i = q_i/q_1$ and

$$I_n^{(1)} = I\left[\alpha+\mu_n^{(1)}, (Y-Y_{ia})/2\sqrt{\beta}\right] \tag{50}$$

$$I_n^{(2)} = I\left[\alpha+\mu_n^{(1)}, (Y-Y_{ib})/2\sqrt{\beta}\right] \tag{51}$$

$$I_m^{(3)} = I\left[\alpha+\mu_m^{(2)}, (Y-Y_{ia})/2\sqrt{\beta}\right] \tag{52}$$

$$I_m^{(4)} = I\left[\alpha+\mu_m^{(2)}, (Y-Y_{ib})/2\sqrt{\beta}\right] \tag{53}$$

and if $X_{ia} < X \leq X_{ib}$,

$$I(A,B) = \frac{1}{A}\left\{\exp\left[-A(X - X_{ia})\right] \operatorname{erf}\left(B/\sqrt{X - X_{ia}}\right)\right\} - \frac{1}{2A}\left\{\exp(2B\sqrt{A}) \operatorname{erfc}\left[\sqrt{A(X - X_{ia})}\right.\right.$$

$$\left.\left. + B/\sqrt{X - X_{ia}}\right] + \exp(-2B\sqrt{A}) \operatorname{erfc}\left[-\sqrt{A(X - X_{ia})} + B/\sqrt{X - X_{ia}}\right]\right\} \tag{54}$$

whereas if $X > X_{ib}$,

$$I(A,B) = \frac{1}{A}\left\{\exp\left[-A(X - X_{ib})\right] \operatorname{erf}\left(B/\sqrt{X - X_{ib}}\right) - \exp\left[-A(X - X_{ia})\right] \operatorname{erf}\left(B/\sqrt{X - X_{ia}}\right)\right\}$$

$$+ \frac{1}{2A}\left(\exp(2B\sqrt{A})\left\{\operatorname{erfc}\left[\sqrt{A(X - X_{ib})} + B/\sqrt{X - X_{ib}}\right] - \operatorname{erfc}\left[\sqrt{A(X - X_{ia})}\right.\right.\right.$$

$$\left.\left.\left. + B/\sqrt{X - X_{ia}}\right]\right\} + \exp(-2B\sqrt{A})\left\{\operatorname{erfc}\left[-\sqrt{A(X - X_{ib})} + B/\sqrt{X - X_{ib}}\right]\right.\right.$$

$$\left.\left. - \operatorname{erfc}\left[-\sqrt{A(X - X_{ia})} + B/\sqrt{X - X_{ia}}\right]\right\}\right) \tag{55}$$

where $C(X,Y,Z)$ is the dimensionless concentration based on the area source strength q_1, that is $C(X,Y,Z) = cK_V/q_1H$. If the area source is at ground level, Z_s is set equal to zero in equations (43) and (44).

Finally, of interest is the solution for an elevated vertical area source, wherein the flux of pollutant from an area in the $x = 0$ plane is specified. This problem may arise in the modeling of an urban plume, where the city is represented as an area source in the $x = 0$ plane that is situated at the downwind end of the area. If the pollutant flux Q_1 (g-sec^{-1}) through an area defined by $-b \leq y \leq b$ and $z_1 \leq z \leq z_2$ is specified, then the boundary condition analogous to equation (25) is

$$c(0,y,z) = \frac{Q_1\, U(b+y)\, U(b-y)\, U(z-z_1)\, U(z_2-z)}{2\bar{u}b(z_2 - z_1)} \tag{56}$$

In dimensionless form, equation (56) becomes

$$C(0,Y,Z) = \frac{U(B+Y)\ U(B-Y)\ U(Z-Z_1)\ U(Z_2-Z)}{2B(Z_2 - Z_1)} \tag{57}$$

where $Z_1 = (z_1 - z_a)/H$, $Z_2 = (z_2 - z_a)/H$, and $B = b/H$.

The solution of equations (31), (33) to (35), and (57) is

$$C(X,Y,Z) = \frac{1}{4B} \exp(-\alpha X)\ \exp\left(-\frac{WZ}{2}\right)\left[\operatorname{erf}\left(\frac{B - Y}{2\sqrt{\beta X}}\right) + \operatorname{erf}\left(\frac{B + Y}{2\sqrt{\beta X}}\right)\right]$$

$$\times \left[\sum_{n=1}^{\infty} \bar{a}_n\, \Phi_n^{(1)}(Z)\ \exp\left(-\mu_n^{(1)} X\right) + \sum_{m=1}^{M} \bar{c}_m\, \Phi_m^{(2)}(Z)\ \exp\left(-\mu_m^{(2)} X\right)\right] \tag{58}$$

where $a_n = I_1/I_2$, $c_m = I_3/I_4$, and

$$I_1 = \frac{1}{\left[\left(\frac{W}{2}\right)^2 + \gamma_n^2\right](Z_2 - Z_1)} \left(\exp\left(\frac{WZ_2}{2}\right)\left\{\frac{W}{2}\left[\cos(\gamma_n Z_2) + \delta_n \sin(\gamma_n Z_2)\right] + \gamma_n\left[\sin(\gamma_n Z_2)\right.\right.\right.$$

$$\left.\left.\left. - \delta_n \cos(\gamma_n Z_2)\right]\right\} - \exp\left(\frac{WZ_1}{2}\right)\left\{\frac{W}{2}\left[\cos(\gamma_n Z_1) + \delta_n \sin(\gamma_n Z_1)\right] + \gamma_n\left[\sin(\gamma_n Z_1)\right.\right.\right.$$

$$\left.\left.\left. - \delta_n \cos(\gamma_n Z_1)\right]\right\}\right) \tag{59}$$

$$I_2 = \frac{1}{2}(1 + \delta_n^2) + \frac{(1 - \delta_n^2)}{4\gamma_n} \sin(2\gamma_n) + \frac{\delta_n}{\gamma_n} \sin^2 \gamma_n \tag{60}$$

$$I_3 = \frac{1}{(z_2 - z_1)}\left(\frac{1}{\frac{W}{2} + \theta_m}\left\{\exp\left[\left(\frac{W}{2} + \theta_m\right)z_2\right] - \exp\left[\left(\frac{W}{2} + \theta_m\right)z_1\right]\right\} - \frac{\tau_m}{\frac{W}{2} - \theta_m}\left\{\exp\left[\left(\frac{W}{2} - \theta_m\right)z_2\right]\right.\right.$$

$$\left.\left. - \exp\left[\left(\frac{W}{2} - \theta_m\right)z_1\right]\right\}\right) \tag{61}$$

$$I_4 = \frac{1}{2\theta_m}\left\{\exp(2\theta_m) - 1 + \tau_m{}^2\left[1 - \exp(-2\theta_m)\right]\right\} - 2\tau_m \tag{62}$$

Secondary particulate matter.- The model developed in the previous section is applicable to gaseous pollutants (with $W = 0$) and to primary particulate pollutants. Analyses of airborne particulate matter have established that a substantial fraction of the particulate matter often cannot be attributable to primary particulate sources but rather is the consequence of conversion of gaseous species to the particulate phase. Obviously sulfate represents one important example of the gas-to-particle conversion. Let us denote by c_p the airborne concentration of a secondary species (such as sulfate) in the particulate phase. Then, the steady-state material balance for this species, analogous to equation (24), is

$$\bar{u}\frac{\partial c_p}{\partial x} - w_s\frac{\partial c_p}{\partial z} = K_H\frac{\partial^2 c_p}{\partial y^2} + K_V\frac{\partial^2 c_p}{\partial z^2} + \nu_g kc - k_p c_p \tag{63}$$

where ν_g is the mass ratio of the secondary particulate species to the primary gaseous species which is being converted and k_p is the first-order rate constant for removal of particulate matter by washout and rainout. In writing equation (63) in this way, the rate constant k_p is taken to represent only the gas-to-particle conversion process and not other scavenging processes.

Since it is assumed that there are no direct sources of the secondary particulate matter, the boundary conditions for equation (63) are

$$c_p(0,y,z) = 0 \tag{64}$$

$$c_p(x,y,z) = 0 \qquad (y \to \pm\infty) \tag{65}$$

$$\frac{\partial c_p}{\partial z} = 0 \qquad (z = H_a) \qquad (66)$$

$$K_V \frac{\partial c_p}{\partial z} + w_s c_p = v_{d,p} c_p \qquad (z = z_a) \qquad (67)$$

where $v_{d,p}$ is the deposition velocity of the particulate matter.

Equations (63) to (67) can be made dimensionless in the same manner as before, where the gaseous emission rate Q_1 is used in the definition of C_p (since there is no direct emission in this case). The result is

$$\frac{\partial C_p}{\partial X} - W \frac{\partial C_p}{\partial Z} = \beta \frac{\partial^2 C_p}{\partial Y^2} + \frac{\partial^2 C_p}{\partial Z^2} + \nu_g \alpha C - \alpha_p C_p \qquad (68)$$

$$C_p(0,Y,Z) = 0 \qquad (69)$$

$$C_p(X,Y,Z) = 0 \qquad (Y \to \pm\infty) \qquad (70)$$

$$\frac{\partial C_p}{\partial Z} = 0 \qquad (Z = 1) \qquad (71)$$

$$\frac{\partial C_p}{\partial Z} = (N_p - W) C_p \qquad (Z = 0) \qquad (72)$$

where $\alpha_p = k_p H^2 / K_V$ and $N_p = v_{d,p} H / K_V$.

It is not possible to obtain readily an analytic solution of equation (68) because of the presence of $C(X,Y,Z)$ accounting for the coupling between the gaseous and particulate phases. Therefore, in studying the behavior of C_p, it is necessary to resort to approximate techniques. Define

$$C_p'(X,Z) = \int_{-\infty}^{\infty} C_p(X,Y,Z)\, dY \qquad (73)$$

$$\bar{C}_p(X) = \int_0^1 \int_{-\infty}^{\infty} C_p(X,Y,Z)\, dY\, dZ \tag{74}$$

$$\bar{C}(X) = \int_0^1 \int_{-\infty}^{\infty} C(X,Y,Z)\, dY\, dZ \tag{75}$$

The integrals C_p', $\bar{C}_p$, and $\bar{C}$ each have an important physical interpretation. The total flow G_g $(g\text{-}sec^{-1})$ of a gaseous pollutant through the plane at any x is given by

$$G_g = \int_{z_a}^{H_a} \int_{-\infty}^{\infty} \bar{u}\, c(x,y,z)\, dy\, dz \tag{76}$$

In dimensionless form (the concentration is based on the source strength Q_1), equation (76) becomes

$$\bar{C}(X) = \frac{G_g}{Q_1} = \int_0^1 \int_{-\infty}^{\infty} C(X,Y,Z)\, dY\, dZ \tag{77}$$

Thus, $\bar{C}(X)$ is the ratio of the mass flow of pollutant at any X to the source strength; $\bar{C}_p(X)$ can be similarly interpreted. Integrals C_p', $\bar{C}_p$, and $\bar{C}$ are also related to the fraction of pollutant lost by deposition, reaction, or rainout and washout. The total mass of pollutant removed by deposition between 0 and x is given by

$$M_d = \int_0^x \int_{-\infty}^{\infty} v_d\, c(x',y,0)\, dy\, dx' \tag{78}$$

which in dimensionless form becomes

$$\frac{M_d}{Q_1} = N \int_0^X C'(X',0)\, dX' \tag{79}$$

Similarly, the fraction of the pollutant removed by first-order reaction M_k/Q_1 is given by

$$\frac{M_k}{Q_1} = \alpha \int_0^X \bar{C}(X')\, dX' \tag{80}$$

Equivalent relationships can be written for the particulate matter.

If one assumes that $C_p'(X,0)$ and $C_p'(X,1)$ can be related to $\bar{C}_p(X)$ in the following approximate way,

$$C_p'(X,0) = f_o\, \bar{C}_p(X) \tag{81}$$

$$C_p'(X,1) = f_1\, \bar{C}_p(X) \tag{82}$$

then one obtains the following equation governing $\bar{C}_p(X)$,

$$\frac{d\bar{C}_p}{dX} + K\bar{C}_p = \nu_g \alpha\, \bar{C}(X) \tag{83}$$

$$\bar{C}_p(0) = 0 \tag{84}$$

where $K = N_p f_o - W f_1 + \alpha_p$. The solution of equation (83) subject to equation (84) is

$$\bar{C}_p(X) = \nu_g \alpha \exp(-KX) \int_0^X \exp(K\xi)\, \bar{C}(\xi)\, d\xi \tag{85}$$

For L point sources of gaseous pollutant, equation (85) becomes

$$\bar{C}_p(X) = \nu_g \alpha \sum_{i=1}^{L} \hat{Q}_i\, U(X-X_i) \left(\sum_{n=1}^{\infty} \frac{a_n \Gamma_n^{(1)}}{K - \left(\alpha + \mu_n^{(1)}\right)} \left\{ \exp\left[-\left(\alpha + \mu_n^{(1)}\right)(X - X_i) \right] - \exp\left[-K(X - X_i)\right] \right\} + \sum_{m=1}^{M} \frac{c_m \Gamma_m^{(2)}}{K - \left(\alpha + \mu_m^{(2)}\right)} \left\{ \exp\left[-\left(\alpha + \mu_m^{(2)}\right)(X - X_i) \right] - \exp\left[-K(X - X_i)\right] \right\} \right) \tag{86}$$

where

$$\Gamma_n^{(1)} = \frac{\exp\left(-\frac{W}{2}\right)\left[\gamma_n(\sin\gamma_n - \delta_n\cos\gamma_n) - \frac{W}{2}(\cos\gamma_n + \delta_n\sin\gamma_n)\right] + \frac{W}{2} + \delta_n\gamma_n}{\left(\frac{W}{2}\right)^2 + \gamma_n^2} \tag{87}$$

and

$$\Gamma_m^{(2)} = \frac{\exp\left(\theta_m - \frac{W}{2}\right) - 1}{\theta_m - \frac{W}{2}} - \frac{\tau_m\left\{1 - \exp\left[-\left(\theta_m + \frac{W}{2}\right)\right]\right\}}{\theta_m + \frac{W}{2}} \tag{88}$$

The assumptions of equations (81) and (82) are difficult or impossible to establish experimentally, and no direct means of estimating the values of f_o and f_1 exist. However, the scaling of the solution and the values of the particulate deposition velocities cause the solution for $\bar{C}_p(X)$ to be quite insensitive to the values of f_o and f_1. If this were not the case, then it would be necessary to consider another means of obtaining a closed form solution for $\bar{C}_p(X)$.

For L area sources, equation (85) can also be evaluated. For $X_{ia} \leqq X \leqq X_{ib}$, the solution is

$$\bar{C}_p(X) = \nu_g\alpha\sum_{i=1}^{L}\hat{q}_i\,U(X-X_{ia})\,(Y_{ib}-Y_{ia})\left(\frac{1-\exp[-K(X-X_{ia})]}{K}\left(\sum_{n=1}^{\infty}\frac{a_n\Gamma_n^{(1)}}{\alpha+\mu_n^{(1)}}\right.\right.$$

$$\left.+\sum_{m=1}^{M}\frac{c_m\Gamma_m^{(2)}}{\alpha+\mu_m^{(2)}}\right) - \sum_{n=1}^{\infty}\frac{a_n\Gamma_n^{(1)}}{\alpha+\mu_n^{(1)}}\left\{\frac{\exp\left[-\left(\alpha+\mu_n^{(1)}\right)(X-X_{ia})\right] - \exp[-K(X-X_{ia})]}{K-\left(\alpha+\mu_n^{(1)}\right)}\right\}$$

$$\left. - \sum_{m=1}^{M}\frac{c_m\Gamma_m^{(2)}}{\alpha+\mu_m^{(2)}}\left\{\frac{\exp\left[-\left(\alpha+\mu_m^{(2)}\right)(X-X_{ia})\right] - \exp[-K(X-X_{ia})]}{K-\left(\alpha+\mu_m^{(2)}\right)}\right\}\right) \tag{89}$$

and for $X \geq X_{ib}$, the solution is

$$\bar{C}_p(X) = \nu_g \alpha \sum_{i=1}^{L} \hat{q}_i \, U(X-X_{ia}) \, (Y_{ib} - Y_{ia}) \left[\frac{1 - \exp\left[-K(X_{ib} - X_{ia})\right]}{K} \left(\sum_{n=1}^{\infty} \frac{a_n \Gamma_n^{(1)}}{\alpha + \mu_n^{(1)}} \right.\right.$$

$$\left. + \sum_{m=1}^{M} \frac{c_m \Gamma_m^{(2)}}{\alpha + \mu_m^{(2)}} \right) + \sum_{n=1}^{\infty} \frac{a_n \Gamma_n^{(1)}}{\alpha + \mu_n^{(1)}} \frac{1}{K - \left(\alpha + \mu_n^{(1)}\right)} \left(\left\{ 1 - \exp\left[-\left(\alpha + \mu_n^{(1)}\right) \right.\right.\right.$$

$$\left.\left.\left. \times (X_{ib} - X_{ia}) \right] \right\} \left\{ \exp\left[-\left(\alpha + \mu_n^{(1)}\right) (X - X_{ib}) \right] - \exp\left[-K(X - X_{ib}) \right] \right\}$$

$$\left. - \left\{ \exp\left[-\left(\alpha + \mu_n^{(1)}\right) (X_{ib} - X_{ia}) \right] - \exp\left[-K(X_{ib} - X_{ia}) \right] \right\} \right)$$

$$+ \sum_{m=1}^{M} \frac{c_m \Gamma_m^{(2)}}{\alpha + \mu_m^{(2)}} \frac{1}{K - \left(\alpha + \mu_m^{(2)}\right)} \left(\left\{ 1 - \exp\left[-\left(\alpha + \mu_m^{(2)}\right) (X_{ib} - X_{ia}) \right] \right\} \right.$$

$$\times \left\{ \exp\left[-\left(\alpha + \mu_m^{(2)}\right) (X - X_{ib}) \right] - \exp\left[-K(X - X_{ib}) \right] \right\}$$

$$\left. \left. - \left\{ \exp\left[-\left(\alpha + \mu_m^{(2)}\right) (X_{ib} - X_{ia}) \right] - \exp\left[-K(X_{ib} - X_{ia}) \right] \right\} \right) \right] \tag{90}$$

Finally, for the elevated area source in the $X = 0$ plane, $\bar{C}_p(X)$ is given by

$$\bar{C}_p(X) = \nu_g \alpha \left(\sum_{n=1}^{\infty} \frac{\bar{a}_n \Gamma_n^{(1)}}{K - \left(\alpha + \mu_n^{(1)}\right)} \left\{ \exp\left[-\left(\alpha + \mu_n^{(1)}\right) X \right] - \exp(-KX) \right\} \right.$$

$$\left. + \sum_{m=1}^{M} \frac{\bar{c}_m \Gamma_m^{(2)}}{K - \left(\alpha + \mu_m^{(2)}\right)} \left\{ \exp\left[-\left(\alpha + \mu_m^{(2)}\right) X \right] - \exp(-KX) \right\} \right) \qquad (91)$$

Equation (91) is of the same form as equation (86) for a single point source at $X = 0$, with $\bar{a}_n$ and $\bar{c}_m$ replacing a_n and c_m in equation (86).

Figure 2 shows $\bar{C}(X)$ as a function of X for a hypothetical point source located at $X = 0.01$, and for $\alpha = N = 1$ (the parameters for SO_2 produce values of α and N of order 1). Figure 2 delineates the various contributions to the decay of the species. For these parameter values both deposition and conversion are important, with deposition more efficient near the source where ground-level concentrations are highest.

REFERENCES

1. Ott, Wayne; and Eliassen, Rolf: A Survey Technique for Determining the Representativeness of Urban Air Monitoring Stations With Respect to Carbon Monoxide. J. Air Pollut. Control Assoc., vol. 23, no. 8, Aug. 1973, pp. 685-690.

2. Roth, P. M.; Reynolds, S. D.; Roberts, P. J. W.; and Seinfeld, J. H.: Development of a Simulation Model for Estimating Ground Level Concentrations of Photochemical Pollutants - Final Report. Rept-71SAI-21, Systems Applications, Inc., 1971. (Available from NTIS as PB 206 415.)

3. Panofsky, Hans Arnold: Objective Weather-Map Analysis. J. Meteorol., vol. 6, no. 6, Dec. 1949, pp. 386-392.

4. Gilchrist, B.; and Cressman, G. P.: An Experiment in Objective Analysis. Tellus, vol. 6, no. 4, Nov. 1954, pp. 309-318.

5. Cressman, George P.: An Operational Objective Analysis System. Mon. Weather Rev., vol. 87, no. 10, Oct. 1959, pp. 367-374.

6. Endlich, R. M.; and Mancuso, R. L.: Objective Analysis of Environmental Conditions Associated With Severe Thunderstorms and Tornadoes. Mon. Weather Rev., vol. 96, no. 6, June 1968, pp. 342-350.

7. Shepard, D.: A Two-Dimensional Interpolation Function for Computer Mapping of Irregularly Spaced Data. TR-15 (Contract N00014-67A-029), Harvard Univ., Mar. 20, 1968. (Available from DDC as AD 668 707.)

8. Shenfeld, L.; and Boyer, A. E.: The Utilization of an Urban Air Pollution Model in Air Management. Air Pollution - Proceedings of the Fifth Meeting of the Expert Panel on Air Pollution Modeling, N. 35, NATO Comm. Challenges Mod. Soc., Aug. 1974, pp. 22-1 - 22-35.

9. Fritsch, J. Michael: Objective Analysis of a Two-Dimensional Data Field by the Cubic Spline Technique. Mon. Weather Rev., vol. 99, no. 5, May 1971, pp. 379-386.

10. MacCracken, M. C.; and Sauter, G. D., eds.: Development of an Air Pollution Model for the San Franscisco Bay Area - Final Report to the National Science Foundation, Volume 1. UCRL-51920 Vol. 1, Lawrence Livermore Lab., Oct. 1, 1975.

11. Anderson, Gerald E.: Mesoscale Influences on Wind Fields. J. Appl. Meteorol., vol. 10, no. 3, June 1971, pp. 377-386.

12. Anderson, G. E.: A Mesoscale Windfield Analysis of the Los Angeles Basin. Environmental Monitoring Series. EPA-650/4-73-001, U.S. Environ. Prot. Agency, June 1973. (Available from NTIS as PB 231 832.)

13. Endlich, Roy M.: An Iterative Method for Altering the Kinematic Properties of Wind Fields. J. Appl. Meteorol., vol. 6, no. 5, Oct. 1967, pp. 837-844.

14. Fankhauser, J. C.: The Derivation of Consistent Fields of Wind and Geopotential Height From Mesoscale Rawinsonde Data. J. Appl. Meteorol., vol. 13, no. 6, Sept. 1974, pp. 637-646.

15. O'Brien, James J.: Alternative Solutions to the Classical Vertical Velocity Problem. J. Appl. Meteorol., vol. 9, no. 2, Apr. 1970, pp. 197-203.

16. Sherman, Christine A.: A Mass-Consistent Model for Wind Fields Over Complex Terrain. UCRL Preprint 76171, Lawrence Livermore Lab., May 1975.

17. Sasaki, Y.: An Objective Analysis Based on the Variational Method. J. Meteorol. Soc. Japan, Ser. 2, vol. 36, no. 3, June 1958, pp. 77-88.

18. Sasaki, Yoshikazu: Some Basic Formalisms in Numerical Variational Analysis. Mon. Weather Rev., Vol. 98, no. 12, Dec. 1970, pp. 875-883.

19. Liu, C. Y.; and Goodin, W. R.: An Iterative Algorithm for Objective Wind Field Analysis. Mon. Weather Rev., vol. 104, no. 6, June 1976, pp. 784-792.

20. Compilation of Air Pollutant Emission Factors (Second Edition). Publ. No. AP-42, U.S. Environ. Prot. Agency, Apr. 1973. (Available from NTIS as PB 223 996.)

21. Bartz, D. R.; Arledge, K. W.; Gabrielson, J. E.; Hays, L. G.; and Hunter, S. C.: Control of Oxides of Nitrogen From Stationary Sources in the South Coast Air Basin of California. KVB 5800-179 (Contract No. ARB 2-1471), Sept. 1974.

22. Hunter, S. C.; and Helgeson, N. L.: Control of Oxides of Sulfur From Stationary Sources in the South Coast Air Basin of California. KVB 5802-432 (Contract No. ARB 4-421), Dec. 1975.

23. Hecht, Thomas A.; and Seinfeld, John H.: Development and Validation of a Generalized Mechanism for Photochemical Smog. Environ. Sci. & Technol., vol. 6, no. 1, Jan. 1972, pp. 47-57.

24. Eschenroeder, Alan Q.; and Martinez, Jose R.: Concepts and Applications of Photochemical Smog Models. Advan. Chem. Ser. No. 113, 1972, pp. 101-168.

25. Hecht, Thomas A.; Seinfeld, John H.; and Dodge, Marcia C.: Further Development of Generalized Kinetic Mechanism for Photochemical Smog. Environ. Sci. & Technol., vol. 8, no. 4, Apr. 1974, pp. 327-339.

26. Whitten, G. Z.; and Hogo, H.: Mathematical Modeling of Simulated Photochemical Smog - Final Report. EPA-600/3-77-011, U.S. Environ. Prot. Agency, June 1975/June 1976. (Available from NTIS as PB 263 348.)

27. Niki, H.; Daby, E. E.; and Weinstock, B.: Mechanisms of Smog Reactions. Adv. Chem. Ser. No. 113, 1972, pp. 16-57.

28. Demerjian, Kenneth L.; Kerr, J. Alistair; and Calvert, Jack G.: The Mechanism of Photochemical Smog Formation. Advances in Environmental Science and Technology, Volume 4, James N. Pitts, Jr., and Robert L. Metcalf, eds., John Wiley & Sons, c.1974, pp. 1-262.

29. Dodge, M. C.: Combined Use of Modeling Techniques and Smog Chamber Data To Derive Ozone-Precursor Relationships. International Conference on Photochemical Oxidant Pollution and Its Control - Proceedings: Volume II, EPA-600/3-77-001b, U.S. Environ. Prot. Agency, Jan. 1977, pp. 881-889. (Available from NTIS as PB 264 233.)

30. Graedel, T. E.; Farrow, L. A.; and Weber, T. A.: Kinetic Studies of the Photochemistry of the Urban Troposphere. Atmos. Environ., vol. 10, no. 12, 1976, pp. 1095-1116.

31. Dodge, M. C.; and Hecht, T. A.: Rate Constant Measurements Needed To Improve a General Kinetic Mechanism for Photochemical Smog. Chemical Kinetics Data for the Upper and Lower Atmosphere, Int. J. Chem. Kinet., Symp. No. 1, 1975, pp. 155-163.

32. Chan, Walter H.; Nordstrom, Robert J.; Calvert, Jack G.; and Shaw, John H.: Kinetic Study of HONO Formation and Decay Reactions in Gaseous Mixtures of HONO, NO, NO_2, H_2O, and N_2. Environ. Sci. & Technol., vol. 10, no. 7, July 1976, pp. 674-682.

33. Fromm, Jacob E.: A Method for Reducing Dispersion in Convective Difference Schemes. J. Comput. Phys., vol. 3, no. 2, Oct. 1968, pp. 176-189.

34. Boris, Jay P.; and Book, David L.: Flux-Corrected Transport. I. SHASTA, a Fluid Transport Algorithm That Works. J. Comput. Phys., vol. 11, no. 1, Jan. 1973, pp. 38-69.

35. Crowley, W. P.: Numerical Advection Experiments. Mon. Weather Rev., vol. 96, no. 1, Jan. 1968, pp. 1-11.

36. Gear, C. W.: Algorithm 407 - DIFSUB for Solution of Ordinary Differential Equations. Commun. ACM, vol. 14, no. 3, Mar. 1971, pp. 185-190.

37. Liu, Mei-Kao; and Seinfeld, John H.: On the Validity of Grid and Trajectory Models of Urban Air Pollution. Atmos. Environ., vol. 9, no. 6/7, June/July 1975, pp. 555-574.

38. Liu, M. K.; Whitney, D. C.; Seinfeld, J. H.; and Roth, P. M.: Continued Research in Mesoscale Air Pollution Simulation Modeling: Volume I - Assessment of Prior Model Evaluation Studies and Analysis of Model Validity and Sensitivity. EPA 600/4-76-016 A, U.S. Environ. Prot. Agency, May 1976. (Available from NTIS as PB 257 526.)

39. Reynolds, Steven D.; Roth, Philip M.; and Seinfeld, John H.: Mathematical Modeling of Photochemical Air Pollution - I. Formulation of the Model. Atmos. Environ., vol. 7, no. 11, Nov. 1973, pp. 1033-1061.

40. Reynolds, Steven D.; Liu, Mei-Kao; Hecht, Thomas A.; Roth, Philip M.; and Seinfeld, John H.: Mathematical Modeling of Photochemical Air Pollution - III. Evaluation of the Model. Atmos. Environ., vol. 8, no. 6, June 1974, pp. 563-596.

41. Reynolds, S. D.; Ames, J.; Hecht, T. A.; Meyer, J. P.; Whitney, D. C.; and Yocke, M. A.: Continued Research in Mesoscale Air Pollution Simulation Modeling: Volume II - Refinements in the Treatment of Chemistry, Meteorology, and Numerical Integration Procedures. EPA 600/4-76-016 B, U.S. Environ. Prot. Agency, May 1976. (Available from NTIS as PB 257 527.)

42. Reynolds, S. D.: The Systems Applications, Incorporated Urban Airshed Model: An Overview of Recent Developmental Work. International Conference on Photochemical Oxidant Pollution and Its Control - Proceedings: Volume II, EPA-600/3-77-001b, U.S. Environ. Prot. Agency, Jan. 1977, pp. 795-802. (Available from NTIS as PB 264 233.)

43. Roth, Philip M.; Roberts, Philip J. W.; Liu, Mei-Kao; Reynolds, Steven D.; and Seinfeld, John H.: Mathematical Modeling of Photochemical Air Pollution - II. A Model and Inventory of Pollutant Emissions. Atmos. Environ., vol. 8, no. 1, Jan. 1974, pp. 97-130.

44. Demerjian, K. L.: Photochemical Air Quality Simulation Modeling: Current Status and Future Prospects. International Conference on Photochemical Oxidant Pollution and Its Control - Proceedings: Volume II, EPA-600/3-77-001b, U.S. Environ. Prot. Agency, Jan. 1977, pp. 777-794. (Available from NTIS as PB 264 233.)

45. Chu, Kuang J.; and Seinfeld, John H.: Formulation and Initial Application of a Dynamic Model for Urban Aerosols. Atmos. Environ., vol. 9, no. 4, Apr. 1975, pp. 375-402.

46. Seinfeld, J. H.; and Ramabhadran, T. E.: Atmospheric Aerosol Growth by Heterogeneous Condensation. Atmos. Environ., vol. 9, no. 12, 1975, pp. 1091-1097.

47. Haagenson, Philip L.; and Morris, Alvin L.: Forecasting the Behavior of the St. Louis, Missouri, Pollutant Plume. J. Appl. Meteorol., vol. 13, no. 8, Dec. 1974, pp. 901-909.

48. Stampfer, J. F., Jr.; and Anderson, J. A.: Locating the St. Louis Urban Plume at 80 and 120 km and Some of Its Characteristics. Atmos. Environ., vol. 9, no. 3, Mar. 1975, pp. 301-313.

49. Breeding, R. J.; Haagenson, P. L.; Anderson, J. A.; and Lodge, J. P., Jr.: The Urban Plume as Seen at 80 and 120 km by Five Different Sensors. J. Appl. Meteorol., vol. 14, no. 2, Mar. 1975, pp. 204-216.

50. Breeding, R. J.; Klonis, H. B.; Lodge, J. P., Jr.; Pate, J. B.; Sheesley, D. C.; Englert, T. R.; and Sears, D. R.: Measurements of Atmospheric Pollutants in the St. Louis Area. Atmos. Environ., vol. 10, no. 4, 1976, pp. 181-194.

51. Bolin, Bert; and Persson, Christer: Regional Dispersion and Deposition of Atmospheric Pollutants With Particular Application to Sulfur Pollution Over Western Europe. Tellus, vol. 27, no. 3, 1975, pp. 281-310.

52. Belot, Y.; Baille, A.; and Delmas, J.-L.: Modele Numerique de Dispersion des Polluants Atmospheriques en Presence de Couverts Vegetaux. Application aux Couverts Forestiers. Atmos. Environ., vol. 10, no. 2, 1976, pp. 89-98.

53. Heines, T. S.; and Peters, L. K.: The Effect of a Horizontal Impervious Layer Caused by a Temperature Inversion Aloft on the Dispersion of Pollutants in the Atmosphere. Atmos. Environ., vol. 7, no. 1, Jan. 1973, pp. 39-48.

54. Scriven, R. A.; and Fisher, B. E. A.: The Long Range Transport of Airborne Material and Its Removal by Deposition and Washout - I. General Considerations. Atmos. Environ., vol. 9, no. 1, Jan. 1975, pp. 49-58.

55. Peterson, Thomas W.; and Seinfeld, John H.: Mathematical Model for Transport, Interconversion, and Removal of Gaseous and Particulate Air Pollutants - Application to the Urban Plume. Atmos. Environ., vol. 11, no. 12, 1977, pp. 1171-1184.

56. Monin, A. S.; and Yaglom, A. M.: Statistical Fluid Mechanics: Mechanics of Turbulence. Volume I. MIT Press, c.1971.

57. Peterson, Thomas William: Aerosol Dynamics in an Urban Atmosphere. Ph. D. Thesis, California Inst. Technol., 1978.

TABLE I.- SOURCES OF INVALIDITY AND INACCURACY IN AIR QUALITY MODELS

Source of error	Comment
Sources of invalidity	
True form of the turbulent fluxes $\overline{u'c_i'}$, $\overline{v'c_i'}$, and $\overline{w'c_i'}$ is unknown.	Higher order closure models will offer improvement over eddy diffusivities in representing these terms. Such closure methods lead to large computational requirements.
Turbulent fluctuating chemical reaction terms are neglected (e.g., eq. (4)).	Closure models appropriate for turbulent chemistry can be developed, but large computational requirements may arise.
Effect of concentration fluctuations from spatial averaging on chemical reaction rate is neglected (e.g., eq. (7)).	Introduce "microscale model" in regions where strong point and line sources occur.
Sources of Inaccuracy	
Mean velocities $\bar{u}$, $\bar{v}$, and $\bar{w}$ are not true ensemble means (usually $\bar{u}$, $\bar{v}$, and $\bar{w}$ are calculated from data at a finite number of locations): Uncertainties in the measurement of wind speed and direction Inadequate or nonrepresentative spatial measurements of wind speed and direction Uncertainties associated with wind field analysis techniques	There is no way to determine the true mean from the data; $\bar{u}$, $\bar{v}$, and $\bar{w}$ can be calculated in principle from accurate fluid mechanical turbulence model.
Source emission function S_i is inaccurate: Inaccurate or no specification of source location Uncertainties in emission factors Inaccurate or no temporal resolution of emission Inadequate or no verification of emission methodologies	More detailed emission inventories are needed to reduce this source of inaccuracy.

TABLE I.- Concluded

Source of error	Comment
Sources of inaccuracy	
Chemical reaction mechanism does not accurately reflect those chemical processes occurring in the atmosphere: Uncertainties in experimental determinations of specific reaction rate constants Variations of rate constants with temperature either uncertain or unknown Inadequacies in lumping due to the nonrepresentativeness of lumped class reactions relative to specific species within the class, for example, reaction rates, products, and stoichiometric coefficients Inaccuracies in the mechanism due to insufficient verification studies	Continued study of chemical processes is needed to insure that R_i is accurate; elimination or quantification of the following smog chamber related errors is also needed: Inadequate or no control and measurement of levels of H_2O in the chamber Impurities in background chamber air Inadequate or no measurements of the spectral distribution and intensity of the chamber irradiation system Inaccurate or ambiguous analytical methods Nonhomogeneity due to inadequate stirring or poor chamber design Adsorption and desorption of reactants and products on chamber walls Chemical reactions occurring on chamber surfaces Inadequate control and measurement of chamber temperature
Boundary conditions are inaccurately specified: Concentrations Inversion height	There is no remedy except for more extensive data.

TABLE II.- COMPARISON OF SAI AND LIRAQ KINETIC MECHANISMS

Reaction	Rate coefficient for -	
	SAI[a]	LIRAQ[b]
NO_x/H_2O chemistry:		
$NO_2 + h\nu \rightarrow NO + O$	Variable	Variable
$O + O_2 + M \rightarrow O_3 + M$	2.08×10^{-5} $ppm^{-2}min^{-1}$	2.16×10^{-5} $ppm^{-2}min^{-1}$
$O_3 + NO \rightarrow NO_2 + O_2$	25.2	26.2
$NO_2 + O \rightarrow NO + O_2$	1.34×10^{4}	1.34×10^{4}
$NO_2 + O_3 \rightarrow NO_3 + O_2$	5.0×10^{-2}	4.35×10^{-2}
$NO_3 + NO \rightarrow 2NO_2$	1.3×10^{4}	1.28×10^{4}
$NO + NO_2 + H_2O \rightarrow 2HONO$	2.2×10^{-9} $ppm^{-2}min^{-1}$	----------
$NO_2 + NO_3 + H_2O \rightarrow 2HONO_2$	1.66×10^{-3} $ppm^{-2}min^{-1}$	----------
$O + NO + M \rightarrow NO_2 + M$	----------	3.41×10^{-3} $ppm^{-2}min^{-1}$
$O + NO_2 + M \rightarrow NO_3 + M$	----------	3.49×10^{-3} $ppm^{-2}min^{-1}$
$NO_3 + NO_2 \rightarrow N_2O_5$	----------	5.59×10^{3}
$N_2O_5 \rightarrow NO_3 + NO_2$	----------	12.2 min^{-1}
$N_2O_5 + H_2O \rightarrow 2HNO_3$	----------	6.84×10^{-6}
$NO_3 + h\nu \rightarrow NO_2 + O$	----------	Variable
NO_x/HO_x chemistry:		
$OH + NO \rightarrow HONO$	9×10^{3}	8.82×10^{3}
$OH + NO_2 \rightarrow HONO_2$	9×10^{3}	1.47×10^{4}
$HO_2 + NO \rightarrow OH + NO_2$	2×10^{3}	4.54×10^{3}
$HO_2 + NO_2 \rightarrow HONO + O_2$	20	----------
$HO_2 + NO_2 \rightarrow HO_2NO_2$	----------	26.2
$HONO + h\nu \rightarrow OH + NO$	Variable	Variable
$CO + OH \rightarrow CO_2 + HO_2$	2.06×10^{2}	2.06×10^{2}

[a]A 31-step mechanism, called the carbon-bond mechanism, has been developed by SAI as a variation of the Hecht-Seinfeld-Dodge mechanism (Whitten and Hogo (ref. 26)). Because of the association of reactions and reactivities with carbon bonds, the range of reactions and the range of rate constants in a kinetic mechanism can be narrowed somewhat if each atom is treated according to its bond type. In this mechanism, hydrocarbons are divided into four groups: single-bonded carbon atoms, fast double bonds (i.e., relatively reactive double bonds), slow double bonds, and carbonyl bonds. Single-bonded carbon includes not only paraffin molecules, but also the single-bonded carbon atoms of olefins, aromatics, and aldehydes. Double bonds are treated as a pair of carbon atoms. An activated aromatic ring is considered as three double bonds in the present formulation of the mechanism, and because of a similarity in reactivities, aromatics are lumped with the slow (ethylene) double bonds rather than with the fast double bonds. In the mechanism HC1, HC2, HC3, and HC4 represent fast double bonds, slow double bonds, single-bonded carbon atoms, and carbonyl bonds, respectively.

[b]In the LIRAQ mechanism HC1 denotes olefins and highly reactive aromatics; HC2, paraffins, less reactive aromatics, and some oxygenates; HC4, aldehydes, some aromatics, and ketones.

TABLE II.- Continued

Reaction	Rate coefficient for -	
	SAI[a]	LIRAQ[b]
$HO_2 + O_3 \rightarrow OH + 2O_2$	----------	1.33
$OH + HO_2 \rightarrow H_2O + O_2$	----------	2.94×10^4
$OH + O_3 \rightarrow HO_2 + O_2$	----------	82.5
$OH + HNO_3 \rightarrow H_2O + NO_3$	----------	1.32×10^2
$O_3 + h\nu \rightarrow O + O_2$	----------	Variable
$O_3 + h\nu + H_2O \rightarrow O_2 + 2OH$	----------	Variable
$HO_2 + HO_2 \rightarrow H_2O_2 + O_2$	4×10^3	4.67×10^3
$H_2O_2 + h\nu \rightarrow 2OH$	Variable	Variable
Hydrocarbon chemistry:		
$HCl + O \rightarrow ROO + RCO_3$	5.3×10^3	4.42×10^{-3}
$HCl + OH \rightarrow ROO + HC4$	3.8×10^4	3.93×10^4
$HCl + OH \rightarrow ROO + H_2O$	----------	1.36×10^4
$HCl + O_3 \rightarrow RCO_3 + OH + HC4$	1.0×10^{-2}	----------
$HCl + O_3 \rightarrow$ OZONIDE	5.0×10^{-3}	----------
$HCl + O_3 \rightarrow HO_2 + RO + HC4$	----------	1.75×10^{-2}
$HCl + NO_3 \rightarrow HC_2 + NO_2$	----------	6.70
$HC2 + O \rightarrow ROO + OH$	----------	57.6
$HC2 + OH \rightarrow ROO + H_2O$	----------	3.23×10^3
$HC2 + OH \rightarrow HC4 + ROO$	8.0×10^3	----------
$HC2 + O \rightarrow RCO_3 + ROO$	37.0	----------
$HC2 + O_3 \rightarrow RCO_3 + HC4 + OH$	2×10^{-3}	----------
$HC2 + NO_3 \rightarrow$ Products	50	----------
$HC3 + O \rightarrow ROO + OH$	20	----------
$HC3 + OH \rightarrow ROO + H_2O$	1.3×10^3	----------
$HC4 + h\nu \rightarrow ROO + OH$	Variable	----------
$HC4 + h\nu \rightarrow CO + H_2$	Variable	Variable
$HC4 + OH \rightarrow RCO_3 + H_2O$	1.0×10^4	6.81×10^3

TABLE II.- Concluded

Reaction	Rate coefficient for -	
	SAI[a]	LIRAQ[b]
$HC4 + h\nu \rightarrow RCO_3 + HO_2$	---	Variable
$HC4 + O \rightarrow OH + RCO_3 + CO$	---	2.30×10^2
$HC4 + HO_2 \rightarrow H_2O_2 + RCO_3$	---	4.77×10^{-3}
$HC4 + RO_2 \rightarrow ROOH + RCO_3$	---	4.03×10^{-3}
$HC4 + NO_3 \rightarrow RCO_3 + HONO_2$	---	0.215
$HC4 + OH \rightarrow CO + H_2O + HO_2$	---	1.36×10^4
Free radical chemistry:		
$NO + ROO \rightarrow RO + NO_2$	---	2.15×10^3
$NO + ROO \rightarrow NO_2 + HC4 + HO_2$	2×10^3	---
$NO_2 + RO \rightarrow RONO_2$	---	2.94×10^3
$NO + RO \rightarrow RONO$	---	2.94×10^3
$NO_2 + RCO_3 \rightarrow PAN$	150	397
$PAN \rightarrow RCO_3 + NO_2$	0.02	---
$NO + RCO_3 \rightarrow ROO + NO_2 + CO_2$	2×10^3	1.07×10^3
$RO + O_2 \rightarrow HO_2 + HC4$	---	0.92
$ROO + HO_2 \rightarrow ROOH + O_2$	4×10^3	3.97×10^3
$ROO + ROO \rightarrow 2RO + O_2$	---	3.97×10^2
$RCO_3 + HO_2 \rightarrow R(O)OOH + O_2$	10^4	---
$RCO_3 + HO_2 \rightarrow ROOH$	---	6.6×10^{-2}
$RCO_3 + RCO_3 \rightarrow HC4$	---	1.47×10^3
Sulfur chemistry:		
$OH + SO_2 \rightarrow OH + SO_4^{=}$	---	8.82×10^2
$RO + SO_2 \rightarrow HO_2 + SO_4^{=}$	---	5.88×10^2
$ROO + SO_2 \rightarrow RO + SO_4^{=}$	---	2.94
$HO_2 + SO_2 \rightarrow OH + SO_4^{=}$	---	1.32

TABLE III.- ATMOSPHERIC AEROSOL SYSTEMS

System	Important mechanisms
Smog chamber	Condensation, coagulation, nucleation, and wall losses
Power plant plume	Convection, diffusion, condensation, coagulation, nucleation, sources, deposition and settling, and washout and rainout
Atmosphere	
Near particulate sources	Condensation, coagulation, nucleation, sources, and deposition and settling
Far from particulate sources	Convection, diffusion, condensation, sources, deposition and settling, and washout and rainout

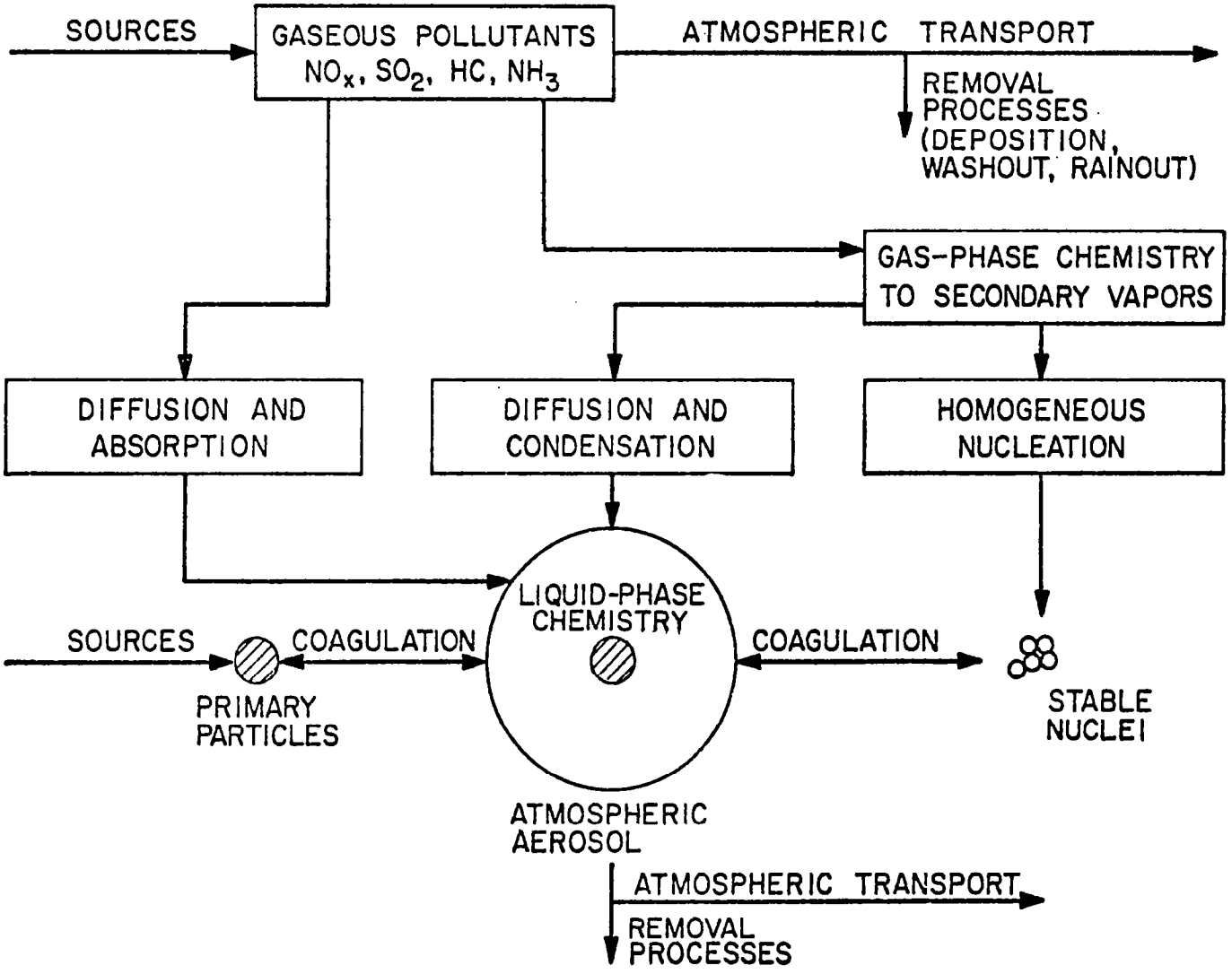

(a) Schematic of complete process.

Figure 1.- Interaction between gaseous and particulate pollutants.

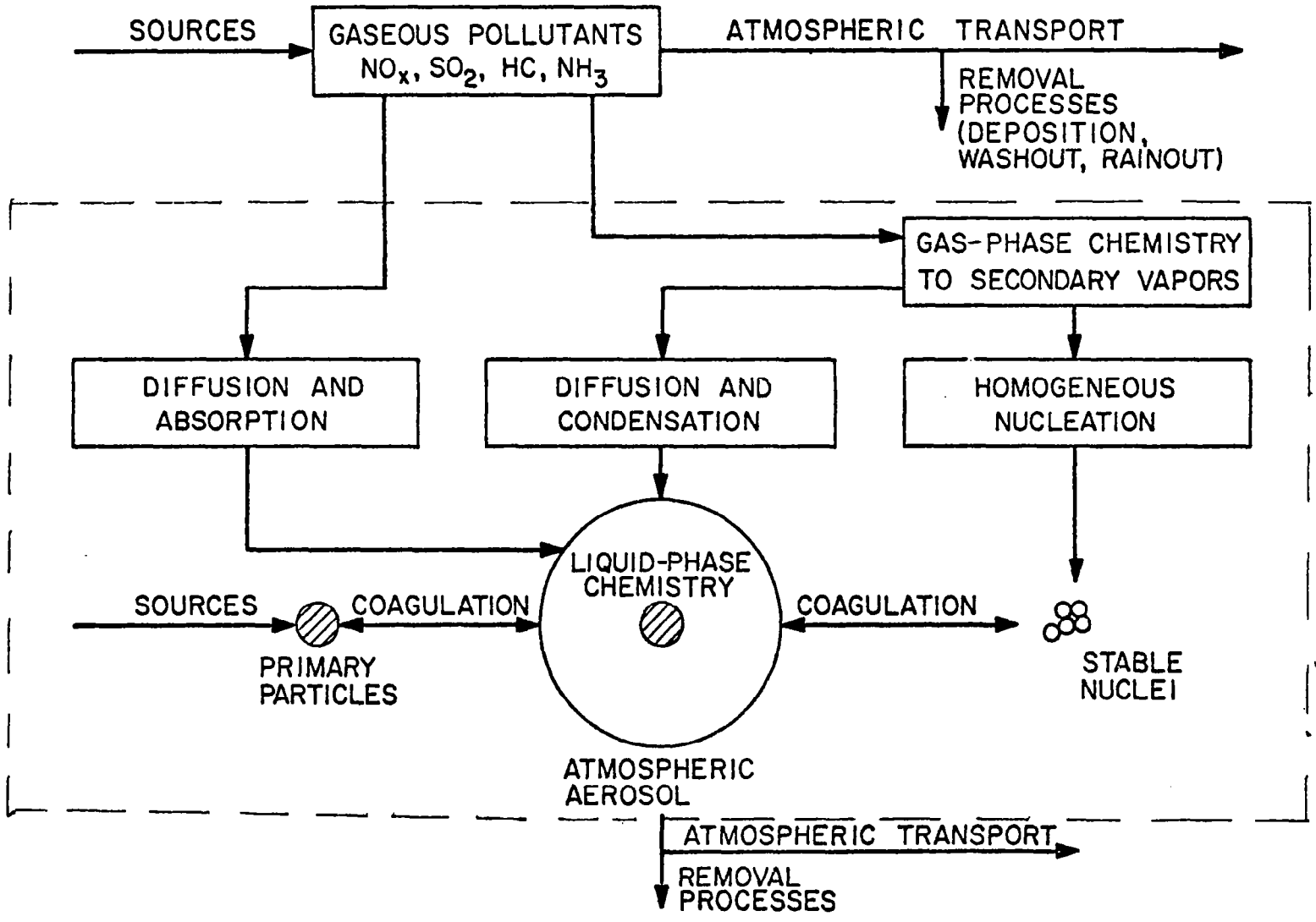

(b) Simple model replaces process within dashed lines.

Figure 1.- Concluded.

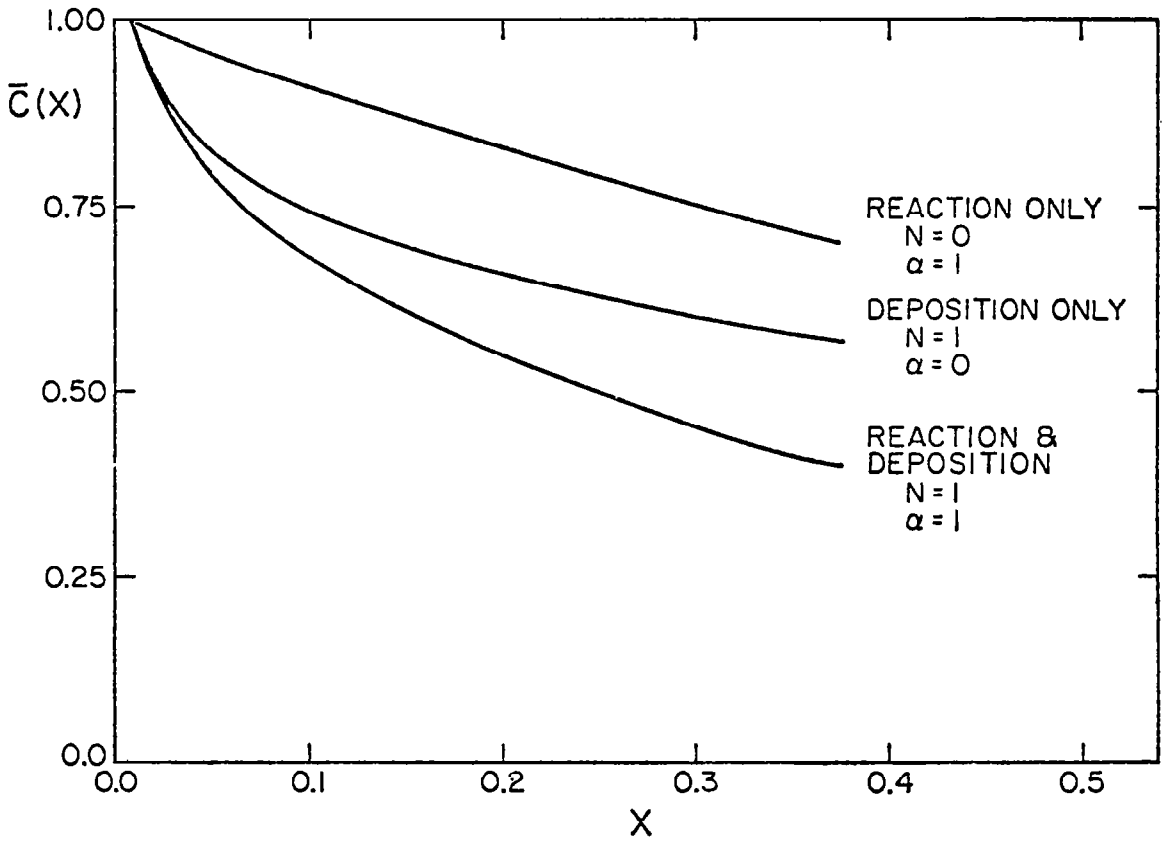

Figure 2.- Relative rates of removal of a gaseous pollutant by reaction and surface deposition.